

NEUTRON AND PHOTON MEASUREMENTS THROUGH CONCRETE
FROM A 15 GEV ELECTRON BEAM ON A TARGET -
COMPARISON WITH MODELS AND CALCULATIONS*

T. M. Jenkins

Radiation Physics Department
Stanford Linear Accelerator Center
Stanford, California 94305

ABSTRACT

Measurements of neutron and photon dose equivalents from a 15 GeV electron beam striking an iron target inside a scale model of a PEP IR hall are described, and compared with analytic-empirical calculations and with the Monte Carlo code, MORSE. The MORSE code is able to predict both absolute neutron and photon dose equivalents for geometries where the shield is relatively thin, but fails as the shield thickness is increased. An intermediate energy source term is postulated for analytic-empirical neutron shielding calculations to go along with the giant resonance and high energy terms, and a new source term due to neutron capture is postulated for analytic-empirical photon shielding calculations. The source strengths for each energy source term, and each type, are given from analysis of the measurements.

Submitted to Nuclear Instruments and Methods

*Work supported by the Department of Energy

I. INTRODUCTION

The Stanford Positron-Electron Project (PEP) now under construction presents some interesting problems in radiation shielding. PEP, a 717 meter diameter storage ring, will have five interaction regions (IR's) where electrons and positrons with energies up to 18 GeV collide. In an effort to learn more about the potential radiation hazards of these interaction areas, a scale model of a PEP IR was assembled in late 1976, and measurements taken under a variety of configurations.

Measurements of radiation levels outside this model of a PEP interaction region hall with a 15 GeV electron beam striking an iron target have been reported recently (AS77) with only spartan editorial comment. The data in that publication include the raw numbers from a moderated BF₃, an Andersson-Braun neutron rem counter, and ion chambers, as well as corrected and reduced data for each. In that form, the data is eminently useful to the various interpreters, the present author being included.

This paper represents an effort to draw together the measurement data, the results for the same geometries of the Monte Carlo computer code, MORSE, and empirical-analytic methods previously used at SLAC for shielding unwanted radiation generated when a high energy electron beam strikes a thick target. In particular, comparisons will be made with PEP-106 (JE74) and PEP-215 (JE76).

The intercomparison of these three utilizes mostly the corrected rem counter and ionization chamber data in reduced form, which is included, along with the reduced BF₃ data, in the appendix.

II. GENERAL COMMENTS ON THE MEASUREMENTS - detectors, locations, etc.

The detectors used in the measurements have been extensively documented (PA65). The moderated BF_3 , a cadmium-lined, 6.2 cm thick polyethylene moderator surrounding a BF_3 gas-filled proportional counter, is a fluence detector for neutrons with energies in the range of a few keV to about 10 MeV. Above some few MeV, the detector response falls off. The actual upper limit of sensitivity is the subject of some uncertainty. Fig. 1, the response as a function of energy as viewed by various authors (MC76) of moderators similar to the one used for these measurements, is given to convey a degree of awareness of the response in the range above a few MeV.

The rem counter, developed by Andersson and Braun (AN64), also has had extensive exposure in the literature. It is a neutron counter with an output tailored to give a rem response in the neutron energy range from thermal to about 7 MeV. The response of this instrument also falls sharply above about 5 MeV (MC76) such that neither this detector nor the moderated BF_3 can be counted on to give trustworthy information above perhaps about 10 MeV. The response of the A-B rem counter is shown as Fig. 2. Despite its limitations, this detector remains one of the better single rem-indicating instruments available to the health physicist.

By combining the fluence and rem data, some information on the average neutron energies and quality factors (in the sensitivity ranges of the instruments) may be deduced (MC76), although it would appear futile unless something were known of the spectral content above 10 MeV.

During the tests reported by Ash, et al., for one of the geometries, the health physics department at LBL made measurements with a bismuth fission chamber, aluminum threshold detectors and a moderated BF₃ detector to derive the integral neutron fluence spectrum and the integral dose spectrum of Fig. 3 (MC76A). While this sounds acceptably elegant, the reader is cautioned that the spectrum was measured only at a single location (8.6 meters from the source, or S3 on the data location chart) and only for one shielding geometry, the so-called '2 foot thick curtain' configuration.

The assumption has subsequently been made, based partly on the relatively constant ratio of rem-BF₃ data, and partly on desperation, that the spectrum doesn't change for all geometries especially where there is at least one foot of concrete between source and detector, and that the total neutron D.E. will be the measured rem counter dose modified to account for that portion of the dose above 10 MeV; that is,

$$\text{D.E. (total neutron)} = \text{D.E. (A-B counter)} / 0.6 \quad (1)$$

These measurements were made in the area just to the east of the experimental hall, ESA, where a concrete tunnel shields the beam transport line for a distance of about 200 feet before it enters the beam dump area buried inside a hill (Fig. 4). The transport pipe was interrupted about 2/3rds of the way to the hill and a thick iron plate inserted. This plate, 8 cm thick, 30 cm wide and about 2 meters in length, was tilted such that the beam struck it at a 4 degree grazing angle in the vertical direction. Shortly downstream of the target, a concrete wall was erected closing off the tunnel simulating the wall that would exist at the entrances to the PEP interaction region halls

from the main storage ring. Measurement locations outside this tunnel in the research area at SLAC are shown in Fig. 4. Not shown on this figure are the measurement locations on top of the roof.

The configuration of the concrete immediately around the target was altered from the basic shape (which had either a 3 or a 5 foot concrete roof) into the four consecutive geometries shown in Fig. 5 to simulate the designs then under consideration for the PEP IR halls. These are shown in more detail in the report by Ash, et al. (AS77). The four geometries were

- (1) the 'open' configuration (roof removed),
- (2) the 'extended wall' configuration (walls extended vertically on three sides, leaving one side at its original height,
- (3) the 'horn' configuration (a 3 foot thick concrete roof placed above the extended walls, completely closing off three sides, and leaving an opening between the top of the original shielding wall and the roof on the fourth side. This simulated a shielding wall in the PEP IR hall that did not extend all the way to the ceiling),
- (4) the 'curtain' configuration (a shielding wall, either one or two feet thick, extended from the top of the open-sided shielding wall to the ceiling to cover the open port).

A comparison of the dimensions of this experimental set-up and the actual PEP interaction region hall shows that we had a reasonable one-third scale model (Fig. 6). Beam height was about 7 feet, the shielding wall height was about 12 feet before being extended, and the thickness of the unextended side walls was about 4 feet.

Composition and density of the concrete weren't measured; it was assumed to be ordinary concrete with an average density of 2.26 g/cm³.

III. GENERAL REMARKS ON PREVIOUS EMPIRICAL-
ANALYTIC SHIELDING METHODS AT SLAC -
including PEP 106 and 215

Shielding methods at SLAC have been covered in numerous previous reports which are referenced in The Stanford Two-Mile Accelerator (NE68). For some expansion, the reader may refer to any of the reports listed in that reference, or to the appendix.

Essentially, we have taken the approach that the radiation patterns outside a shield may be calculated by dividing the problem up into parts, each of which may be described by its own physics. The total dose equivalent then in the sum of each of these parts. These parts are (a) high energy neutrons (HEN); (b) giant resonance neutrons (GR); and (c) photons. That is,

$$\text{D.E. (total)} = \text{D.E. (HEN)} + \text{D.E. (GR)} + \text{D.E. (photons)} \quad (2)$$

A. High Energy Neutrons (T_n>100 MeV)

For high energy neutrons, the D.E. is given by (DE62)

$$\text{D.E. (HEN)} = E_o C \left(\frac{\sin \theta}{a + d} \right)^2 \left(\frac{1}{E_o} \frac{dN}{d\Omega} \right) \exp \left(\frac{-d\rho}{\lambda_1 \sin\theta} \right) \text{ rem/e (3)}$$

where

E_o = beam energy lost in a target, in GeV,

θ = angle from target to measurement point,

d = shield thickness, cm,

ρ = shield density, g/cm³,

a = target-to-shield distance, cm,

λ_1 = removal mean-free path for neutrons, which because the inelastic cross section is constant above about 100 MeV, is assumed to be constant. For earth, the value of λ is 117 g/cm²; for concrete, $\lambda = 120$ g/cm² (G166, page 113),

C = fluence-to-dose conversion factor, which also is assumed to be constant after the first few layers of a shield at about 1.15×10^{-7} rem per n/cm² (JE74),

$1/E_0 \, dN/d\Omega$ = yield of neutrons with energies, T_n , greater than 100 MeV per GeV electron, shown in Fig. 7 (DE77). DeStaebler has fit this yield with the analytic expression

$$\frac{1}{E_0} \frac{dN}{d\Omega} = \frac{1.5 \times 10^{-4}}{(1-0.72 \cos\theta)^2} \text{ n/sr-GeV-e} \quad (3A)$$

Combining the various constants allows Eqn. 3, with the answer in rem/e, to be given as

$$\text{D.E. (HEN)} = \frac{1.73 \times 10^{-11} E_0 (\sin \theta)^2 \exp(-d\rho/\lambda_1 \sin \theta)}{(1-0.72 \cos \theta)^2 (a+d)^2} \quad (3B)$$

The maximum D.E. from these neutrons will occur, not directly above the source, but at some angle which is a function of the shield thickness (see Fig. 8). The dose maxima can be seen to shift toward 90° as the shield thickness increases. The point of maximum D.E. as a function of production angle for $T_n > 100$ MeV and for $T_n > 150$ MeV is shown as Fig. 9 (DE77).

The value of the dose maximum relative to the 90° dose is given in Fig. 10 as a function of shield thickness. Thus one may elect to calculate the dose at 90° and then determine the value and point of the dose maximum using Figs. 9 and 10.

The D.E. outside a shield from high energy neutrons at 90° is

$$D.E. (HEN) = \frac{1.73 \times 10^{-11} E_0}{(a + d)^2} \exp\left(\frac{-d\rho}{\lambda_1}\right) \text{ rem/e} \quad (4)$$

It is possible, within a limited range of angles, to calculate doses along the shield as a function of the angle measured from a target that has been abstracted directly under the point of dose maximum, and using the 90° value for the yield at all angles. This simple model is shown in Fig. 8 for two shield thicknesses as dashed lines.

B. Giant Resonance Neutrons ($T_n < 20$ MeV)

The yield of GR neutrons per GeV electron may be described by (SW77)

$$Y = E_0 1.49 \times 10^{-2} Z^{0.73} \text{ n/GeV-e} \quad (5)$$

This yield is isotropic leading to a D.E. of

$$D.E. (GR) = \frac{YCE_0}{4\pi} \left(\frac{\sin\theta}{a+d}\right)^2 \exp\left(\frac{-d\rho}{\lambda_2 \sin\theta}\right) \text{ rem/e} \quad (6)$$

where E_0 is in GeV, C = fluence-to-dose conversion factor, about 3.2×10^{-8} rem per n/cm², and λ_2 = about 30 g/cm² for concrete. Combining constants, this becomes (with the answer in rem/e)

$$D.E. (GR) = 3.79 \times 10^{-11} E_0 \left(\frac{\sin\theta}{a+d}\right)^2 Z^{0.73} \exp\left(\frac{-d\rho}{\lambda_2 \sin\theta}\right) \text{ rem/e} \quad (6A)$$

For an iron target ($Z=26$) at 90° , the GR neutron D.E. becomes

$$D.E. (GR) = \frac{4.09 \times 10^{-10} E_0}{(a + d)^2} \exp\left(\frac{-d\rho}{\lambda_2}\right) \text{ rem/e} \quad (7)$$

(The constant previously used in Eq. 7 (JE76) was 5.07×10^{-10} based on

earlier data.)

C. Photons

There are two essential features of the photon shielding calculations at SLAC. First, the electron beam is assumed to strike a thick target at a shallow (glancing) angle which produces the largest ionizing doses in the direction of the open face (JE70) while at the same time producing a maximum yield of neutrons; and second, the energy is assumed to be carried by photons with energies at the Compton minimum for the target material (NE66). Also, for purposes of this report, rads and rems will be assumed to be equal for photon doses, and all photon doses will be given in units of rems.

The shielding of photons may be approached in a manner analogous to high energy neutrons because the assumption is made that the mass attenuation coefficient (analogous to the removal mean-free path for HEN's) is constant with the value at the Compton minimum. Thus, the D.E. for photons from high energy electrons may be given by

$$\text{D.E. (photons)} = E_0 C \left(\frac{\sin \theta}{a + d} \right)^2 \left(\frac{1}{E_0} \frac{dN}{d\Omega} \right) B(\theta) \exp \left(\frac{-\mu}{\rho} \frac{\rho d}{\sin \theta} \right) \text{ rem/e} \quad (8)$$

where

μ/ρ = mass attenuation coefficient, which because the energy is carried by photons with energies at the Compton minimum, is assumed to be constant. In concrete, the value of μ/ρ (assuming 8 MeV photons, Compton minimum in iron) is $0.024 \text{ cm}^2/\text{g}$.

C = fluence-to-dose conversion factor, which also is assumed to

be constant after the first few layers of a shield at about 2.14×10^{-9} rem per photon/cm² (IC21),

$B(\theta)$ = a build-up factor (G054), energy and material dependent,

$\frac{1}{E_0} \frac{dN}{d\Omega}$ = yield of photons of all energies from electromagnetic shower theory. For the actual spectrum at any given angle, a computer code such as EGS (F077) would be used. For production angles between 10 and 180 degrees, we have fit the yield of photons by the expression

$$\frac{1}{E_0} \frac{dN}{d\Omega} = \frac{0.83}{(1-0.98 \cos\theta)^{1.2}} \text{ photons/sr-GeV-e} \quad (8A)$$

Combining the various constants in Eq. 8 then gives (in rem/e)

$$\text{D.E. (photons)} = \frac{1.78 \times 10^{-9}}{(1-0.98 \cos\theta)^{1.2}} E_0 \left(\frac{\sin\theta}{a+d} \right)^2 B(\theta) \exp\left(\frac{-\mu}{\rho} \frac{d\rho}{\sin\theta} \right) \quad (8B)$$

for production angles between 10 and 180 degrees.

Fig. 11 shows the dose transmitted through concrete of varying thickness as a function of production angle using Eq. 8B with $B(\theta)=1$. Again, as in the neutron case, a shifting of the point of maximum dose toward 90° is seen with increasing shield thickness. Also included as dashed lines are the doses using the simple model.

Ionizing doses, measured for different angles of incidence of a 2 GeV beam, are shown normalized to 1 GeV in Fig. 12 (JE70). These measurements were made in open air with TLD's which responded to ionizing radiation of very low energies as well as higher energies (that is, it includes contributions, not only of high and low energy photons, but also electrons and other ionizing particles). Subsequent calculations, using the Monte Carlo computer code, EGS, give the rela-

tive rad doses from both the photon component, and electrons and positrons for 1.5 degree incident angle, and shown as broken lines in Fig. 12. It is apparent from this figure that electrons-positrons will dominate doses especially at the larger angles ($\theta > 15$ degrees) whenever there is no shield between source and observer.

EGS gives the average energy of the large angle e^+/e^- ($\theta > 60$ degrees for the case of an input electron energy of 15 GeV at 1.5 degrees) as about 5 MeV, with few or no particles whose energies are greater than 15 MeV (at the larger angles). From Feather's rule ($R = 0.542E - 0.133$ in g/cm^2) the range of 5 MeV electrons in concrete is about 1.14 cm, where the density of SLAC concrete is $2.26 g/cm^3$. Thus, the electrons will be removed in the first few centimeters of shielding material.

From a simple shielding standpoint therefore, the upper measured curve (which is also the sum of the EGS e^+/e^- and γ dashed curves) would be used for a no-shield geometry, while the lower dashed curve (photon only) would be used for thickness of shielding beyond the range of the electrons. The 1.5 degree targeting curve has been used simply because no one can predict at what angle a beam might strike a component, and we happen to have measurements at that angle. The value of the photon dose at 90° per GeV would be 1.8×10^{-9} rem-cm²/Gev-e.

The dose through a shield at 90° then is given by

$$D.E. \text{ (photons)} = \frac{1.78 \times 10^{-9} E_0}{(a+d)^2} B(\theta) \exp\left(\frac{-\mu}{\rho} \rho d\right) \text{ rem/e} \quad (9)$$

The transmission of the ionizing component through concrete and other media were reported in a DESY publication (DI76) for a similar

geometry experiment. Two figures modified from that report are included here as Figs. 13 and 14. The latter, which includes the transmission through ordinary concrete, covers the range of thicknesses from 0 to about 80 cm. Figs. 13 and 14 have been modified to show dose in $\text{rem-cm}^2/\text{GeV-e}$ scaling from the DESY measurements done at 7.2 GeV, 200 cm from the source, and for 10^{11} electrons, and setting rads and rems equal.

The DESY measurements were made with an incident beam angle of 2 degrees compared to 4 degrees at SLAC, and with an iron target 0.2 cm thick compared with an 8 cm thick target at SLAC.

There is some question as to whether a build-up factor, and if so, which one should be used when calculating transmission through a medium. (The problem doesn't exist for Monte Carlo calculations; the discussion here is limited to empirical-analytic methods.) Using the EGS code, Nelson (NE77) was able to show that there is a build-up of sorts for bremsstrahlung from thin targets struck by electrons with energies up to a few tens of MeV, but the build-up is extremely small, and noticeable only at very small thicknesses. In Figs. 13 and 14, we can see that the photon doses are completely swamped at the small thicknesses by other ionizing radiation, presumably mostly electrons and positrons, and so no effects of build-up can be detected.

Whether or not one elects to use a build-up factor then is probably not an important criteria as long as the source term is adjusted and the correct value of the mass attenuation coefficient, μ/ρ , used that fits the measured data. The μ/ρ value for concrete from the DESY data in Fig. 14 in the range of 30 to 80 cm thicknesses, is $0.0240 \text{ cm}^2/\text{g}$

and the source term, determined from the zero intercept, is about 5.6×10^{-11} rem-cm²/GeV-e.

This same data can be fit by a single slope with an 8 MeV build-up factor removed. For subsequent calculations using an 8 MeV build-up, one would then have a different source term, 5×10^{-11} rem-cm²/GeV-e, and a value for μ/ρ of 0.0294 cm²/g.

Having thus noted that the use of a build-up factor is somewhat arbitrary for our purposes as long as the correct source and μ/ρ values are used, we shall restrict ourselves to examining the SLAC ionizing data without the build-up factor.

D. Total Doses

Eq. 2 for the total D.E. now becomes the sum of Eqs. 3B, 6A and 8B

$$\begin{aligned} \text{D.E.} = & 10^{-11} E_o \left(\frac{\sin\theta}{a+d} \right)^2 \left[\frac{1.73}{(1-0.72\cos\theta)^2} \exp \left(-\frac{d\rho}{\lambda_1 \sin\theta} \right) \right. \\ & + 3.79 Z^{0.73} \exp \left(-\frac{d\rho}{\lambda_2 \sin\theta} \right) \\ & \left. + \frac{178}{(1-0.98\cos\theta)^{1.2}} \exp \left(\frac{-\mu}{\rho} \frac{\rho d}{\sin\theta} \right) \right] \text{ rem/e} \end{aligned} \quad (10)$$

At 90 degrees using an iron target, this becomes

$$\begin{aligned} \text{D.E. (Total)} = & 10^{-11} E_o \left[1.73 \exp \left(\frac{-d\rho}{\lambda_1} \right) \right. \\ & \left. + 40.9 \exp \left(\frac{-d\rho}{\lambda_2} \right) + 178 \exp \left(\frac{-\mu}{\rho} d\rho \right) \right] \text{ rem/e} \end{aligned} \quad (10A)$$

E. Empirical-Analytic Methods for Shielding Radiation Inside a Large Structure

The experience at SLAC with this type of problem has been confined to measurements with PuBe sources at various heights above the ground,

and some duct measurements inside the accelerator tunnels. The literature on ducting is fairly extensive, but is addressed mostly to ducts with small cross-sectional areas and to energies well below SLAC-PEP design. Measurements in ducts have been reported from high energy proton accelerators (ST73), but again have been isolated to small tunnels, and these measurements don't include the ionizing component found at electron accelerators. Thus, it remains to be seen whether one of the computer codes can be used for this application.

IV. MONTE CARLO COMPUTER CODES, PARTICULARLY MORSE

For the transport of radiation through thick shields, a high energy transport code, such as HETC (CH72) or FLUTRA(RA71), normally would be used. These codes, however, are not very efficient in following scattering inside tunnels or large rooms, particularly when the major component of scattering will come from lower energy neutrons. A code more suited to this would be the three-dimensional Monte Carlo code, MORSE (ST70), which does handle neutrons with energies below about 20 MeV, and photons with energies below about 14 MeV. An obvious deficiency in this code for our purposes is its inability to handle radiation with energies above about 20 MeV. Ultimately, a coupling of codes such as HETC and MORSE will be required for a complete solution.

MORSE is a multipurpose neutron and gamma-ray transport Monte Carlo code where the solution of neutron, gamma-ray, or coupled neutron, gamma-ray problems may be obtained in either the forward or the adjoint mode. General three-dimensional geometry may be used with an albedo option at any material surface, which makes the code well suited geo-

metrically for the PEP problems.

One deficiency of a computer code of this type is the so-called 'deep penetration' problem where the code is apt to give either misleading information, or else the variance becomes too large, and the user must employ variance reduction techniques (such as path-length stretching, source energy and direction biasing, etc.). For most of the PEP shielding applications, we are already in the deep penetration region both for photons and for giant resonance neutrons. Thus, one must be extremely careful with this code when either the shield becomes fairly thick (for example, beyond 60 cm for neutrons and about 30 cm for photons) or where the variance becomes quite large for other reasons and the total doses begin to approach the direct doses, indicating incorrect results (AN69)).

For a neutron source term, the measurements and calculations of several authors (SW76) were combined in Fig. 15, where the data points are from 30 MeV electrons or bremsstrahlung on Pb and Al, 234 MeV on Pb, 150 MeV on Ta, 85 MeV on Fe and 45 MeV on Pb, with different target thicknesses. This was fit by the analytic expression

$$\frac{dN}{dE} = \frac{k (E)^{1/2}}{\left[1 + \left(\frac{E}{2}\right)^{4/3}\right]^3} \quad (11)$$

with $k=3$, and shown by the solid line in the figure.

For a photon source spectrum, both an 8 MeV monoenergetic photon and a complete spectrum generated by the Monte Carlo code, EGS (F077), were used. For this latter, 15 GeV electrons were made to strike a thick iron target at a glancing angle of 1.5 degrees. The resultant spectrum at 74 degrees is shown as Fig. 16.

Tissue response functions used in MORSE were taken from ICRP 21, and are given in the appendix along with the various source spectra used as inputs to MORSE.

Finally, the composition of concrete is that given in NCRP 38, with a value for calcium added by its relative value given in an early report by Wallace (WA62). This is also included in the appendix. The density of concrete used at SLAC is assumed to be 2.26 g/cm^3 .

V. RESULTS

Most of the measurement locations were selected, not for determining D.E. through the thicker shields, but for determining the overall radiation patterns for these particular geometries, and to compare these patterns with the computer code, MORSE. MORSE was not expected to be a candidate for determining radiation D.E.'s through the thicker shields because of the dominance of source terms outside the limits of MORSE in producing the expected D.E.'s. Thus, the measurements on the 3 and 5 foot thick roofs will be compared with analytic-empirical models, while the doses at the side locations (including the vertical measurements), and at long distances from the target, will be compared with MORSE.

A. Neutron Measurements

1. Roof

For neutron D.E., the data from the rem counter, corrected to give total D.E., will be examined first. The transmission through ordinary concrete, and also the value of the source terms for each of the neutron energy regions (high energy and giant resonance) may be

determined by examining the neutron D.E. at the various roof positions.

Of the side positions at the nominal measurement height of 3-6 ft., the data from position S1 can be included for determining transmission (at all distances further from the thick side shield, doses from the relatively thin curtains dominate). Also vertically, the data from S19 16 and S19 20 can be used because these have a direct line-of-sight to the target. Absorption of the neutrons in the iron target will be accounted for only for the measurement in the horizontal target plane where there is appreciable target material; somewhat arbitrarily, the thickness will be chosen as 10 cm allowing a few cm for shower development. The value of λ_1 , removal mean-free-path for high energy neutrons, is 145 g/cm^2 in iron. Only high energy neutrons are considered for this position because the lower shielding wall is already 4 feet thick where only these neutrons will penetrate and add to the measured dose equivalent.

Next, the data from the 3 and 5 foot thick roofs is normalized to a 90° yield by using Eqn. 3B. Finally, all the D.E.'s thus derived are multiplied by R^2 (source-to-detector distances), and plotted as Fig. 17.

The following observations have been made from this figure. First, the data does follow a somewhat orderly drop-off, which is satisfying. However, attempting to fit the measured curve with only the two slopes corresponding to 120 g/cm^2 for HEN's and 30 g/cm^2 for GR neutrons doesn't quite work. This gives a GR neutron source yield that is almost an order of magnitude too high, which we do not expect, and the sum curve still doesn't fit the measured curve too well. Therefore, a third slope is postulated which, in the real physical world,

corresponds to those neutrons in the energy region between 20 and 100 MeV. Actually, we were always acutely aware of these neutrons, but because they exist in a region where the inelastic cross section is rapidly changing, and because the magnitude of a single source term chosen to account for all neutrons within this intermediate energy range was unknown, they were not included. These neutrons will be important in the intermediate shield thickness region (i.e., between 50 and 100 cm of concrete); at smaller thicknesses, the GR neutrons dominate, and at larger thickness, high energy neutrons dominate. From Fig. 17, a value of λ for these intermediate energy neutrons that gives a good fit to the measured data is 55 g/cm^2 .

Other observations from this figure are the values of the source terms (yields times fluence-to-dose conversion factors) for each of the three energy regions derived from the zero intercepts. These values, at an electron energy of 15 GeV (in $\text{rem-cm}^2/15 \text{ GeV-e}$), are

$$\text{G.R. neutrons} = 6.2 \times 10^{-9} \text{ (the value previously used)}$$

$$\text{MID. neutrons} = 1.5 \times 10^{-9} \text{ (not previously included)}$$

$$\text{H.E. neutrons} = 1.5 \times 10^{-10} \text{ (0.6 of the value previously used)}$$

(The difference from calculation in the high energy source term is probably due to the choice of fluence-to-dose conversion factor previously used, or in the assumptions based on the constancy of the integral dose spectrum for all geometries, and not in the actual yield of neutrons.)

More universally, the source terms at 90° per GeV source electron would be

$$GR = 4.09 \times 10^{-10} \text{ rem/GeV-e}$$

$$MID = 1.00 \times 10^{-10} \text{ rem/GeV-e}$$

$$HEN = 1.00 \times 10^{-11} \text{ rem/GeV-e}$$

Thus, we now modify Eqn. 10 to include a mid-energy term, and adjust the values of the various constants. To do this, an angular dependence for the mid-energy term must be included. Somewhat arbitrarily, this will be an analytic fit to those neutrons with energies greater than 25 MeV given in the reference by NEAL (NE68, page 1038),

$$\frac{1}{E_0} \frac{dN}{de} = \frac{3.13 \times 10^{-3}}{(1-0.75\cos\theta)} \text{ n/sr-GeV-e} \quad (12)$$

with a fluence-to-dose conversion factor of 3.2×10^{-8} rem/n/cm². This leads to a revised expression for neutrons which now includes three energy terms,

$$\begin{aligned} \text{D.E. (neutron)} = & 10^{-11} E_0 \left(\frac{\sin\theta}{a+d} \right)^2 \left[\frac{\exp\left(\frac{-dp}{\lambda_1 \sin\theta}\right)}{(1-0.72\cos\theta)^2} \right. \\ & + 10 \frac{\exp\left(\frac{-dp}{\lambda_3 \sin\theta}\right)}{(1-0.75\cos\theta)} \\ & \left. + 3.79 Z^{0.73} \exp\left(\frac{-dp}{\lambda_2 \sin\theta}\right) \right] \text{ rem/e} \quad (13) \end{aligned}$$

The absolute comparisons between calculations and measurements on top of the 3 and 5 foot thick roofs are shown next in Fig. 18. There are three different sets of data on this figure. First are shown actual measurement points, squares or circles (where the uncertainties

are about 8-15% per data point) (AS77) along the roof. The second, shown as dashed lines, are the doses calculated from Eqn. 3B using high energy neutrons only. The third, shown as solid lines, are from calculations using all three energy terms, Eqn. 13.

Good agreement can be seen using the three energy neutron source term, Eqn. 13. The agreement is not as close using only the high energy neutron yield, but is still within a factor of 1.5 for all measurement angles.

2. Side Positions

MORSE was scaled essentially to include the tunnel, its various configurations, the concrete pad, and the hills that surround the research area. Vertical locations were chosen for each of S1 through S4, and a single height only in the horizontal plane at about 3 feet above the ground, for the other further locations. The comparison, on an absolute scale, for the open, extended wall, horn and two curtain geometries is shown in Figs. 19 through 21. For the two foot curtain, (Fig. 21), the component of D.E. coming directly through the 4 foot thick side shield (measured when the 5 foot thick roof was in place), was subtracted to determine only that part of the measured D.E.'s coming from the curtains.

Fig. 22 is included to show how well MORSE also predicts the vertical radiation patterns for the one foot thick curtain configuration. The H.E.-produced component of the dose coming through the thick side wall has been subtracted from the data, but is included as a dashed line on the data at 2.85 m. It did not add to the doses at the further locations.

These figures illustrate how well MORSE is able to predict the patterns of neutron D.E. for these geometries even though the source term in MORSE is not the actual (or complete) source term from the experiment.

Those who have used MORSE understand that the output, using the 'point estimator' is given in fluence, or D.E., per incident source particle. For the absolute comparison to have been made, the yield of source neutrons per incident high energy electron had to be known. We could not simply use the giant resonance value of 0.16 n/GeV-e (or 2.4 neutrons per electron for this test done at 15 GeV) because the other energy neutrons (so-called mid, and high energy) will interact in the concrete walls to produce lower energy neutrons, which in turn will appear as G.R. neutrons in the measurement. In fact, this test will allow an 'apparent' source yield to be determined that can be used in MORSE for these geometries. The apparent yield of neutrons per electron is given on each of the Figs. 19-21, and is also plotted in Fig. 23 as a function of curtain thickness. This last figure (Fig. 23) indicates that MORSE can be used for a similar geometry with curtain thicknesses up to one foot with a single source term, but beyond this thickness an adjustment must be made in the apparent source term. Beyond 2 feet curtain thickness, MORSE no longer will give useful answers for a high energy electron source.

B. PHOTON and Other Ionizing Radiation Measurements

1. Roof

The initial attempt will be made to reduce the photon data using

the same techniques as were used with the neutron data, with a few exceptions.

The data at the side positions, S1 at the 6, 16 and 20 foot heights, was used for the neutron study simply because of the dominance of the high energy neutrons in producing the measured D.E.'s at those positions. Photons, however, are much more sensitive to the proper choice of iron thickness, and also almost no photons will be transmitted through the thick lower side wall. Thus, only the data from the roof positions, corrected for source angular dependence using Eqn. 8B, will be used to determine dose transmission. The results are multiplied by R^2 and plotted as Fig. 24.

No clear pattern emerges from Fig. 24 as was the case with the neutron data. A single slope, corresponding to a $(\frac{H}{\rho})^{-1}$ of 42 g/cm² (solid line) with a zero intercept of 2×10^{-8} rem-cm² per 15 GeV-e (about 3/4th's of the expected value) is a poor fit at best. A case might be made for a tailing off of the data at the larger concrete thicknesses from this figure, perhaps due to the effects of neutron inelastic collisions or capture of the evaporation neutrons produced from high energy neutrons inside the concrete. This has been added as the dashed line in Fig. 23, with a zero intercept (or source term) of 4×10^{-11} rem-cm²/15 GeV-e, or 2.67×10^{-12} rem-cm² per GeV-e.

The rationale for including this term comes from examining the data at some great depth, 200 cm for example. At this depth, the measured neutron D.E. is 3×10^{-12} rem-cm²/15 GeV-e. HEN's will produce evaporation neutrons which give rise to most of the expected photon dose from neutrons (primarily through capture). The number of gamma

rads per neutron rad will depend upon where in the shield the neutrons lie, but may be anywhere between 1/2 and 5, for example (NC71). The ratio of rem-to-BF3 was constant on the roof at about 3.8×10^{-8} rem per unit fluence, which can be interpreted as representing an average energy of between 1 and 2 MeV, and a Q.F. of 10. Thus the measured neutron rad dose would be 3×10^{-13} rad-cm²/15 GeV-e at this depth. Applying the photon per neutron number of between 1/2 and 5 from above would give values of neutron-produced photon doses between 1.5×10^{-13} and 1.5×10^{-12} rem-cm²/15 GeV-e. The value selected from Fig. 24 is about 7×10^{-13} rem-cm²/15 GeV-e, within predicted limits.

Thus, Eq. 8B is now modified to include this possible high energy neutron-generated term, and at the same time the constant is adjusted giving

$$\begin{aligned}
 \text{D.E. (photon)} = 10^{-11} E_o \left(\frac{\sin\theta}{a+d} \right)^2 & \left[\frac{133 \exp \left(\frac{-\mu}{\rho} \frac{d\rho}{\sin\theta} \right)}{(1-0.98 \cos\theta)^{1.2}} \right. \\
 & \left. + \frac{0.267 \exp \left(\frac{-d\rho}{\lambda_1 \sin\theta} \right)}{(1-0.72 \cos\theta)^2} \right] \text{ rem/GeV-e}
 \end{aligned} \tag{14}$$

where λ_1 is the same as defined for high energy neutrons.

The absolute comparisons are now made with the roof data in Fig. 25 where again there are three different sets of data. First, actual measurement points are shown as circles or squares where the errors are somewhat uncertain. (The ionizing data was taken with a portable survey meter reading rate information during the measurement cycles.) Second, shown by the dashed lines, is Eq. 8B, with the constant adjusted to 1.33×10^{-9} . Finally, Eq. 14 which includes the effects of the high energy term and with the constant also adjusted, is

shown as the solid lines.

Neither Eq. 8B nor 14 is adequate in predicting the measured effects, though the shape and amplitude are good for both. The measured positions of the dose maxima are shifted downstream of the calculated positions. It is difficult to ascribe this to a steering error because of other measurements which are more orderly. At the same time, the photon spectrum isn't changing dramatically within the angles of interest (30 to 130 degrees) such that the positional shift could be ascribed to a hardening of the spectrum at the forward angles. Finally, there is some response of the ion chambers to neutrons, but this effect can be shown to be only about 10 percent of the observed readings, and thus can't explain the shift in position of the observed dose maxima.

Thus, somewhat ruefully, we conclude that a simple analogue treatment of photon doses through concrete in a geometry similar to this, must await a better experiment. In the meantime, Eq. 14 will be used to describe doses outside shielding with an appropriate shifting in position of the calculated points.

We should point out that there is considerable difference between the DESY and SLAC photon yields per GeV (5.5×10^{-11} vs. 1.33×10^{-9} rem-cm²/GeV-e) which is due presumably to the difference in iron target thicknesses (0.2 cm at DESY versus 8 cm at SLAC). Also, for very thin or no shield geometries, electrons and positrons must be taken into account when calculating ionizing radiation. Using the EGS calculations at large output angles (74-90 degrees for an incident 15 GeV beam at 1.5 degrees), the electron-positron doses are some 20 times greater than the photon doses. On the other hand, the electron-

positron dose measured at DESY is a factor of 270 greater than the photon dose. The higher $e^{+,-}/\gamma$ ratio at DESY must be due to the thin target which allows the maximum number of e^+/e^- 's to escape the surface, but does not allow for the complete electromagnetic shower development. For a thick target as at SLAC, only those electrons near the surface will escape. If the $e^{+,-}/\gamma$ factor of 20 is applied to the SLAC measured photon yield at zero shield thickness, the e^+/e^- source term becomes

$$\begin{aligned} \text{Dose (electrons)} &= (1.33 \times 10^{-9}) \quad (20) \\ &= 2.66 \times 10^{-8} \quad \text{rad-cm}^2/\text{GeV-e} \quad (15) \end{aligned}$$

This is quite close to the DESY value of 1.5×10^{-8} rad-cm²/GeV-e of Fig. 14. Thus, for calculational purposes, the dose yield of Eq. 15 would be applied for no shielding geometries, and with these electrons attenuated out very quickly, as shown in Fig. 14, or calculated by Feather's rule for a few MeV electrons.

2. Side Positions

As in the case of neutrons, MORSE was not used for transmission through the thicker shields, i.e., the 3 and 5 foot roof thicknesses, but was run for the four test geometries as shown in Figs. 26 and 27. Again, we note reasonable fidelity in MORSE producing the measured doses at different distances from the source for all three geometries. The apparent photon yields per 15 GeV electron (the numbers needed to normalize MORSE to measurements) vary from about 1700 γ/e (horn), 2500 γ/e (ext. wall), to 4700 γ/e for the curtain and 7700 γ/e for the open configuration. (These are also included in Fig. 23 as apparent photons per GeV-e).

This is to be compared with an absolute yield of photons into a 30 degree cone about 90° of 2100 γ/e as determined by EGS for a 15 GeV electron at 1.5 degrees into a thick iron target.

While MORSE can be used to predict photon doses for these geometries, using the apparent yields of Fig. 23, its usefulness for photons would seem to be severely limited with a high energy electron source. At the lower end of concrete thicknesses (up to 30 cm), electrons-positrons dominate the measured doses, and these aren't included in MORSE. At the other end (above 60 cm or so), MORSE is laboring (the deep penetration problem), and neutron-produced gamma doses from high energy neutrons not included in MORSE come into effect. Thus its utility is questionable for photons using high energy electrons as a source.

VI. SUMMARY

Before attempting a summary, it might be worth while reiterating a few of the basic assumptions that have been made about the source and data. Briefly, these are

- 1) The electron beam impinges upon a thick, medium Z target (iron in these tests) at a shallow angle producing the maximum ionizing doses in the direction of the open target face (vertical for this test), and also developing the shower sufficiently to give maximum neutron doses;
- 2) The observed radiation patterns, both neutron and photon, can be scaled directly with electron beam energy, such that inter-comparisons are possible with similar data at different

energies;

- 3) The total observed neutron D.E.'s for the SLAC measurements are the D.E.'s measured with the A-B rem counter divided by 0.6 to account for neutrons above the energy range of this detector. This will be true, under our assumptions, for each of the test geometries;
- 4) When examining the photon (ionizing radiation) data, and comparing it with data taken elsewhere, rad and rem doses are assumed to be equivalent;
- 5) MORSE will be a viable code to use with a high energy electron source in a scattering environment because of the dominance of lower energies in producing doses, both neutron and photon, for thin to intermediate shield thicknesses. It is of questionable utility for thick shields.

For simple shielding geometries, such as shielding a source with an overfill or cover, an analytic expression that includes three source terms for the neutron component and two terms for the photon component gives excellent results for intermediate shielding thicknesses, i.e., 30-200 cm concrete, particularly for neutrons. This expression is of the form

$$\text{D.E. (total)} = \text{D.E. (neutron)} + \text{D.E. (photon)}$$

where the D.E. (neutron) is given by Eq. 13, and the D.E. (photon) is given by Eq. 14, and with the added precaution that the location of the photon equivalent points may be shifted in position from those measured in this experiment.

That is,

$$\begin{aligned}
 \text{D.E. (neutron)} = & 10^{-11} E_o \left(\frac{\sin\theta}{a+d} \right)^2 \left[\frac{\exp \left(\frac{-d\rho}{\lambda_1 \sin\theta} \right)}{(1-0.72 \cos\theta)^2} \right. \\
 & + \frac{10}{(1-0.75 \cos\theta)} \exp \left(\frac{-d\rho}{\lambda_3 \sin\theta} \right) \\
 & \left. + 3.79 z^{0.73} \exp \left(\frac{-d\rho}{\lambda_2 \sin\theta} \right) \right] \text{ rem/e} \quad (13A)
 \end{aligned}$$

and

$$\begin{aligned}
 \text{D.E. (photon)} = & 10^{-11} E_o \left(\frac{\sin\theta}{a+d} \right)^2 \left[\frac{133 \exp \left(\frac{-\mu}{\rho} \frac{d\rho}{\sin\theta} \right)}{(1-0.98 \cos\theta)^{1.2}} \right. \\
 & \left. + \frac{0.267 \exp \left(\frac{-d\rho}{\lambda_1 \sin\theta} \right)}{(1-0.72 \cos\theta)^2} \right] \text{ rem/Gev-e} \quad (14A)
 \end{aligned}$$

MORSE still remains the best candidate for use with complex geometries where scattering must be accounted for, and that's what the experiment was really all about. It has been shown to give good results in the SLAC geometries, except for the thicker shields. Because of the uncertainty that would exist in the 'apparent source' term, its use would seem to be restricted to geometries similar to the mock-up used in these tests.

ACKNOWLEDGEMENTS

The author wishes to thank Dr. H. DeStaebler for many helpful discussions, to Dr. W. R. Nelson for help with the EGS code, and to J. B. McCaslin for a helpful reading of the text.

REFERENCES

- AN64 I.O. Andersson and J. Braun, A Neutron Rem Counter, A E-132, 1964.
- AR69 T. W. Armstrong and P. N. Stevens, A V^0 Importance Function for the Monte Carlo Calculation of the Deep Penetration of Gamma-Rays, J. Nucl. Eng., 23, 331, (1969).
- AS77 W. Ash, et al, PEP Radiation Shielding Tests in SLAC A-Beam, SLAC TN-77-5, (1977).
- CH72 K. C. Chandler and T. W. Armstrong, "Operating Instructions for the High-Energy Nucleon-Meson Transport Code, HETC, ORNL-4744, Oak Ridge National Laboratory, (1972).
- DE62 H. DeStaebler, Jr., Transverse Radiation Shielding for the Stanford Two-Mile Accelerator, SLAC-9, (1962).
- DE77 H. DeStaebler, Jr., Private Communication, (1977).
- DI76 H. Dinter and K. Tesch, Measurements of Dose and Shielding Parameters of Electron-Photon Stray Radiation from a High-Energy Electron Beam, Nucl. Inst. & Meth., 143, (1977).
- F077 R. L. Ford and W. R. Nelson, The EGS Code System: Computer Programs for the Monte Carlo Simulation of Electromagnetic Cascade Showers, to be published, (1977).
- GI66 W. S. Gilbert, et al, 1966 CERN-LRL-RHEL Shielding Experiment at the CERN Proton Synchrotron, UCRL-17941, (1966).
- G054 H. Goldstein and J. E. Wilkins, Calculations of the Penetration of Gamma-Rays, USAEC Report NYO-3075, (1954).
- IC21 ICRP Publication 21, Data for Protection against Ionizing Radiation from External Sources, (1971).
- JE70 T. M. Jenkins, G. J. Warren and J. L. Harris, Angular Distribution of Radiation from a Collimator, a Thick Plate and a Thin Plate

- Struck by a 2 GeV Electron Beam, SLAC TN-70-34, (1970).
- JE74 T. M. Jenkins, J. B. McCaslin and R. H. Thomas, Shielding Required for Radiation Produced by 15 GeV Stored Electrons, PEP 106, (1974).
- JE76 T. M. Jenkins, PEP 215 (1976).
- KA72 K. R. Kase and W. R. Nelson, Concepts of Radiation Dosimetry, SLAC-153, (1972).
- LI61 S. J. Lindenbaum, Shielding of High-Energy Accelerators, Ann. Rev. Nucl. Sci., 11, (1961).
- MC76 J. B. McCaslin, et al, An Intercomparison of Dosimetry Techniques in Radiation Fields at Two High-Energy Accelerators, Health Physics, 33, (1977).
- MC76A J. B. McCaslin, et al, Neutron Spectral Measurements for PEP Interaction Region Mockup Experiment, H. P. Note 68, (1976).
- MO61 B. J. Moyer, Evaluation of Shielding Required for the Improved Bevatron, UCRL-9769, (1961).
- NC71 NCRP Report 38, Protection Against Neutron Radiation, (1971).
- NE68 R. B. Neal, ed., "The Stanford Two-Mile Accelerator," W. A. Benjamin, New York, (1968).
- NE66 W. R. Nelson, et al, Electron-Induced Cascade Showers in Copper and Lead at 1 GeV, Phys. Rev., 149, (1966).
- NE77 W. R. Nelson, private communication.
- PA65 H. Wade Patterson, Accelerator Radiation Monitoring and Shielding UCRL-16445, (1965).
- PA73 H. Wade Patterson and R. H. Thomas, Accelerator Health Physics Academic Press, New York, (1973).
- PR57 B. T. Price, C. C. Horton and K. T. Spinney, Radiation Shielding, Pergamon Press, New York, (1957).

- RA71 J. Ranft and J. T. Routti, FLUKA and MAGKA, Monte Carlo Programs for Calculating Nucleon-Meson Cascades in Cylindrical Geometries, CERN Internal Report LABII-RA/71-4, (1971).
- ST73 G. R. Stevenson and D. M. Squier, "An Experimental Study of Attenuation of Radiation in Tunnels Penetrating the Shield of an Extracted Beam of the 7 GeV Proton Synchrotron Nimrod," Health Physics, 24, 87, (1973).
- ST70 E. A. Straker, et al, The Morse Code - A Multigroup Neutron and Gamma-Ray Monte Carlo Transport Code, ORNL-4585, (1970).
- SW76 W. P. Swanson, Radiation Parameters for Electron Linear Accelerators, (to be published).
- SW77 W. P. Swanson, Calculation of Neutron Yields Released by Electrons incident upon Selected Materials, SLAC-PUB-2042, (1977).
- WA62 R. Wallace and C. Sondhaus, Techniques Used in Shielding Calculations for High-Energy Accelerators: Applications to Space Shielding, UCRL-10439, (1962).

FIGURE CAPTIONS

1. Response of moderated BF_3 detector as a function of energy (MC76).
2. Response of A-B rem counter as a function of energy (MC76).
3. Integral neutron fluence and dose spectra for 2 foot curtain.
Measurement made at location S3. (MC76A)
4. Research area at SLAC showing side locations (roof locations not shown). Letters refer to compass points.
5. Geometries used for PEP mock-up tests. Not shown are initial geometries with 3 or 5 foot roofs covering the target.
6. Outlines of the test and the design of a PEP IR hall. The PEP design is about 3 times the mock-up test dimensions.
7. Yield of high energy neutrons from electrons. Yield shown for neutrons with energies, T_n , > 100 and 150 MeV.
8. Calculated neutron D.E.'s outside varying thicknesses of concrete as a function of production angle, θ_m . Solid line from Eq. 3B; dashed line from simple model.
9. Maximum D.E. outside a shield versus production angle from high energy neutrons and photons.
10. Correction factor for maximum D.E. relative to 90 degrees.
11. Calculated photon doses through varying thicknesses of concrete as a function of production angle. Solid lines from Eq. 8B and attenuation for 8 MeV photons; dashed line from simple model.
12. Ionizing doses from 2 GeV electrons onto a thick target normalized to 1 GeV. Measurements at 1.5 and 3 degree targeting angle.
(Solid line through data points fit by eye.); histograms from EGS calculations at 1.5 degrees.

13. Photon dose per GeV-e through Pb and Fe (DI77).
14. Photon dose per GeV-e through sand and concrete (DI77). Dashed line for $\mu/\rho = 0.0240 \text{ cm}^2/\text{g}$.
15. GR neutron spectrum from various authors. Dashed line from Eq. 11.
16. Calculated photon spectrum at 74 degrees from EGS for 15 GeV electrons on Fe at 1.5 degrees. Dashed line = fit by eye.
17. Measured total neutron D.E.'s for 3 and 5 foot roof positions and selected side locations. Solid lines = slopes for $\lambda_2 = 30 \text{ g/cm}^2$ (GR), $\lambda_3 = 55 \text{ g/cm}^2$ (mid) and $\lambda_1 = 120 \text{ g/cm}^2$. Dashed line = composite curve.
18. Total neutron D.E.'s on top of 3 and 5 foot roofs. Solid line from Eq. 13; Dashed line = from Eq. 3B with HEN's only.
19. Absolute comparison of neutron measurements (data points) with MORSE calculations (solid lines) for the horn and extended wall geometries.
20. Absolute comparison of neutron measurements (data points) with MORSE calculations (solid lines) for the open and 1 foot thick curtain geometries.
21. Absolute comparison of neutron measurements and MORSE for the 2 foot thick curtain geometry. The direct component through the 4 foot thick side wall, measured when the 5 foot roof was in place, has been subtracted to give the data points.
22. Absolute comparison of vertical neutron measurements (data points) and MORSE (solid lines) for the 1 foot curtain geometry at locations S1, S2, S3 and S4. Open squares = Before subtraction of direct component.

23. Apparent yields per electron per GeV for MORSE versus curtain thickness.
24. Measured photon doses for the 3 and 5 foot roof positions. Solid line for $\mu/\rho = 0.0240 \text{ cm}^2/\text{g}$ ($\lambda = 42 \text{ g/cm}^2$). Dashed line for $\lambda_1 = 120 \text{ g/cm}^2$ matched to the photon data at about 220 cm concrete thickness. Dotted line = composite curve.
25. Photon doses on 3 and 5 foot roofs. Solid line from Eq. 14. Dashed line = from Eq. 8B with attenuation for 8 MeV photons.
26. Absolute comparison of photon measurements (data points) with MORSE (solid lines) for the horn and extended wall geometries.
27. Absolute comparison of photon measurements (data points) with MORSE for the open and 1 foot thick curtain geometries.

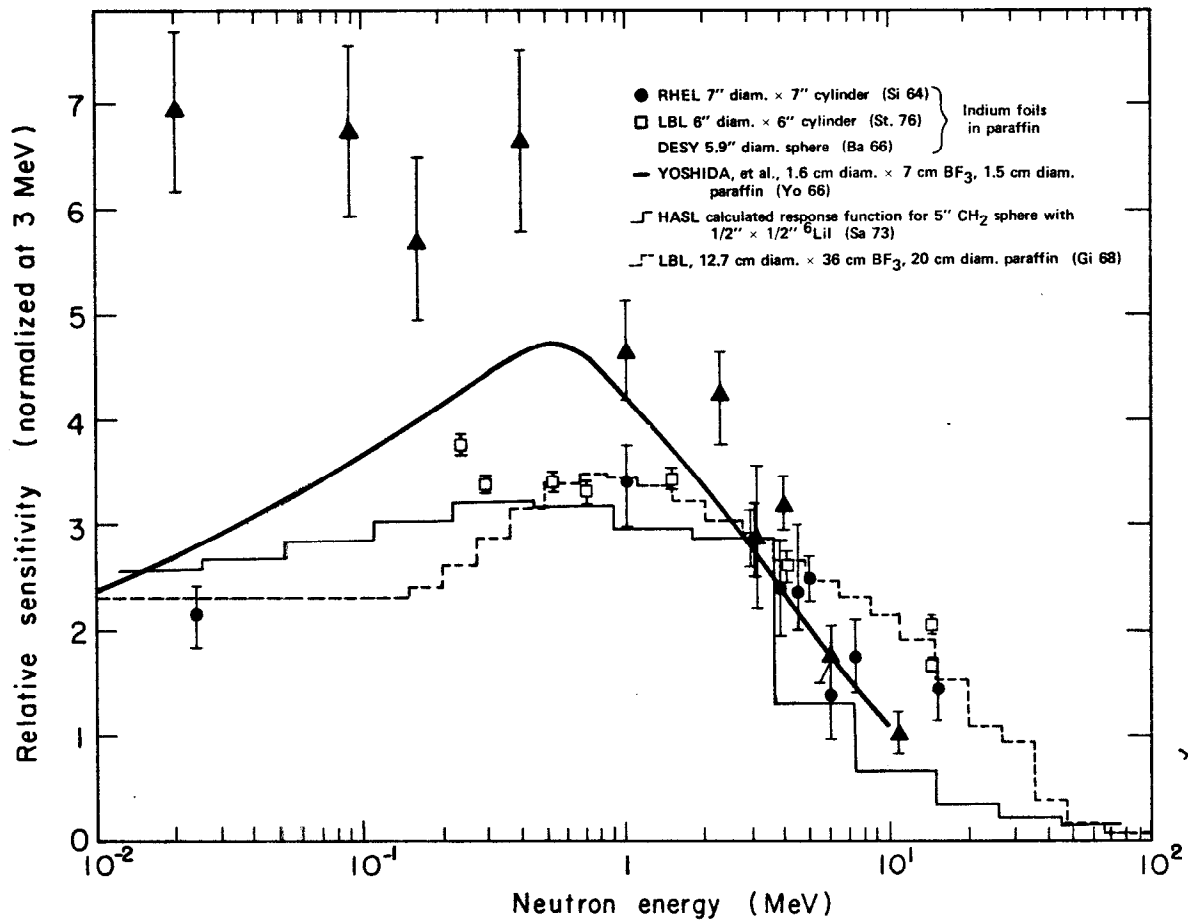


Fig. 1

XBL 769 - 3955

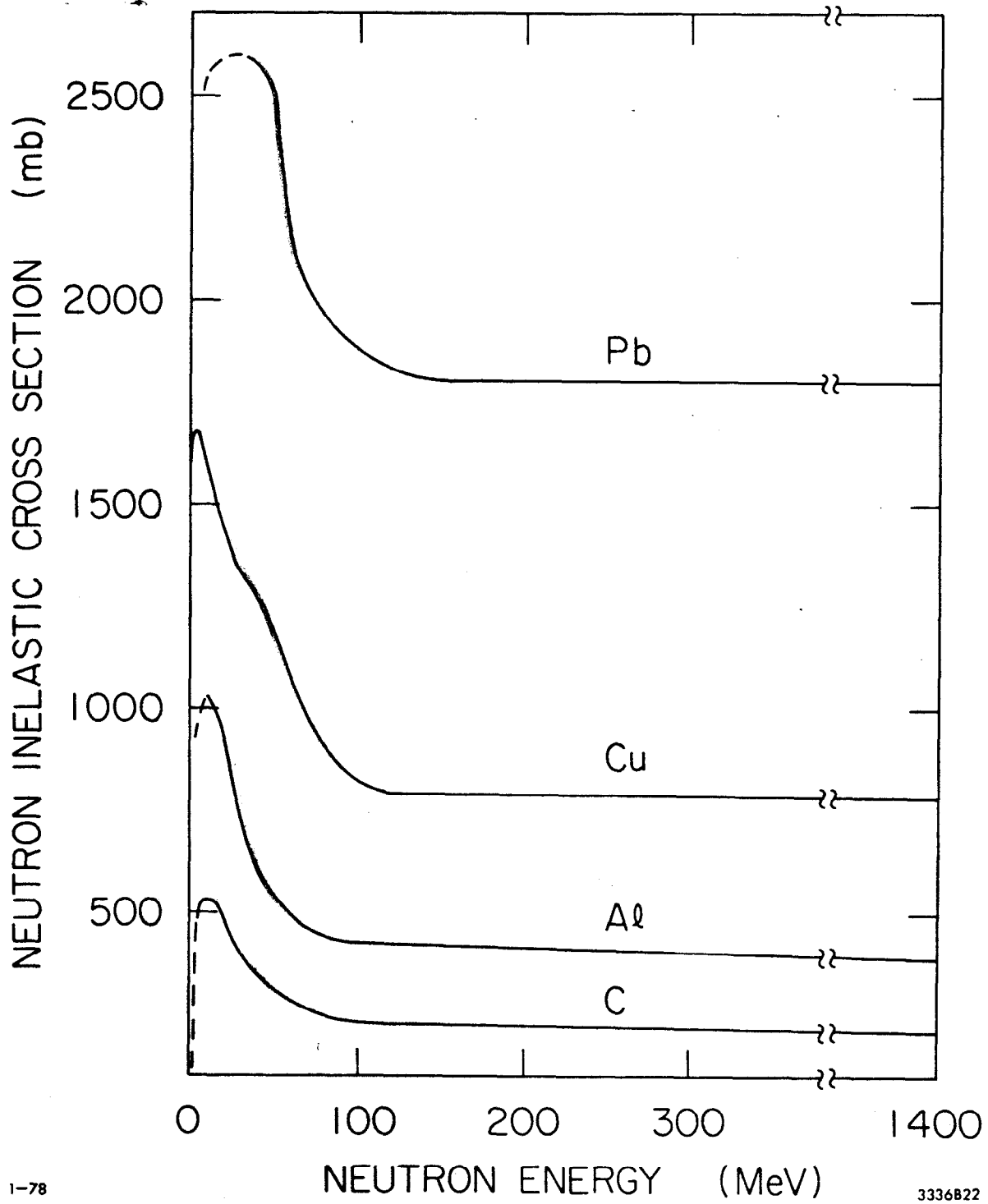


Fig. 1A

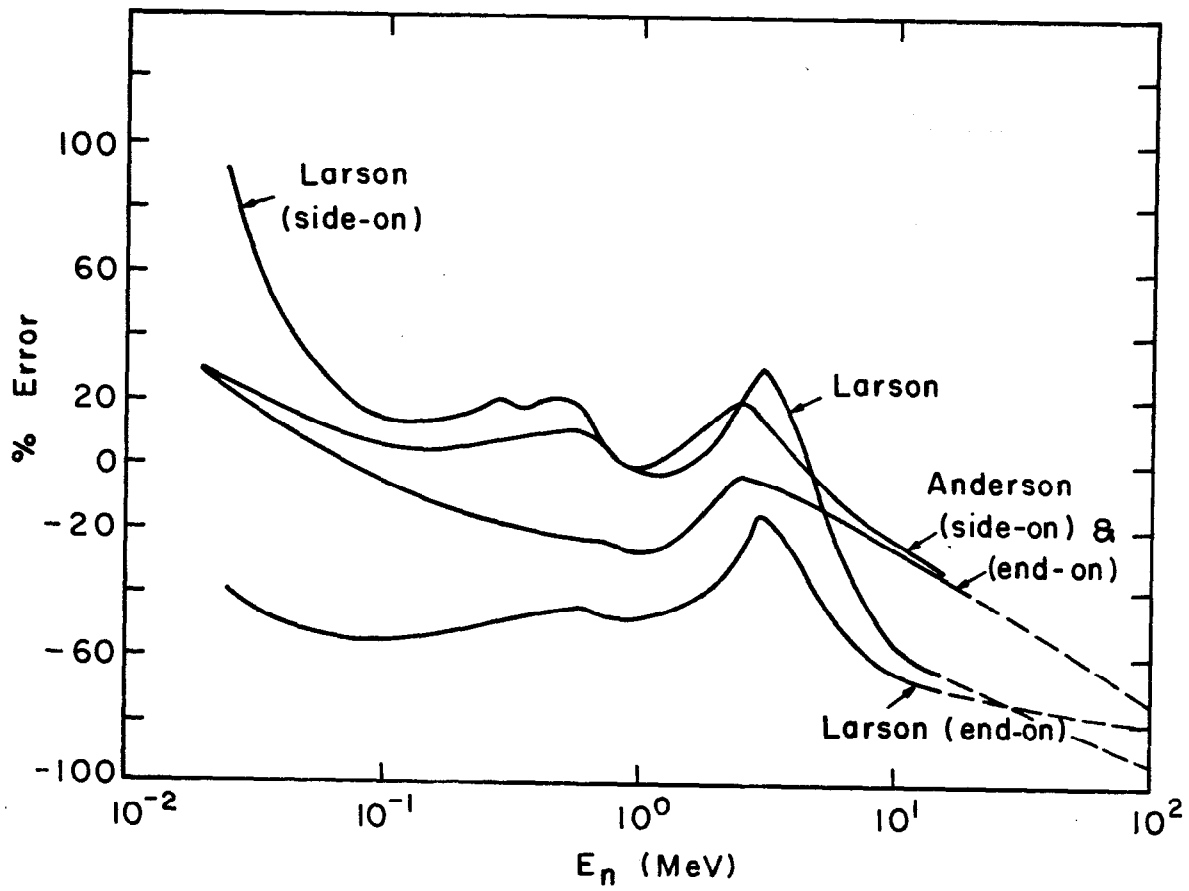


Fig. 2

XBL751-2074

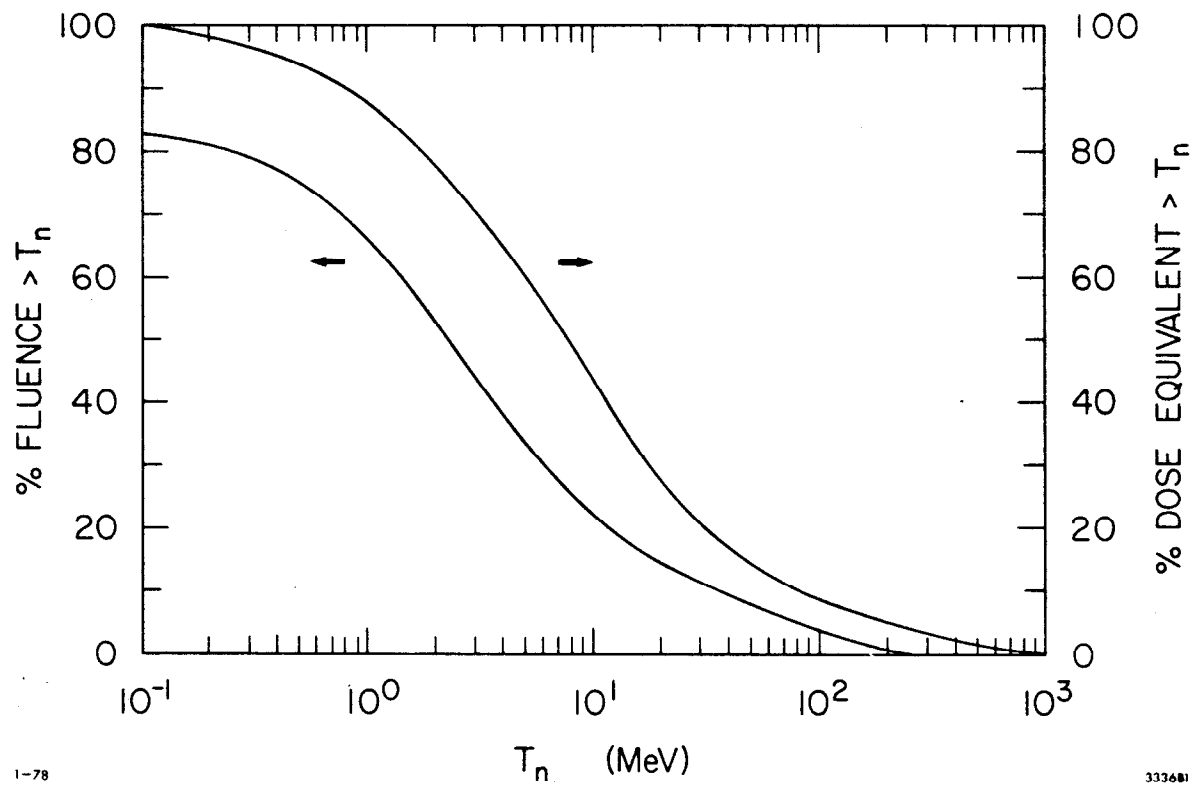
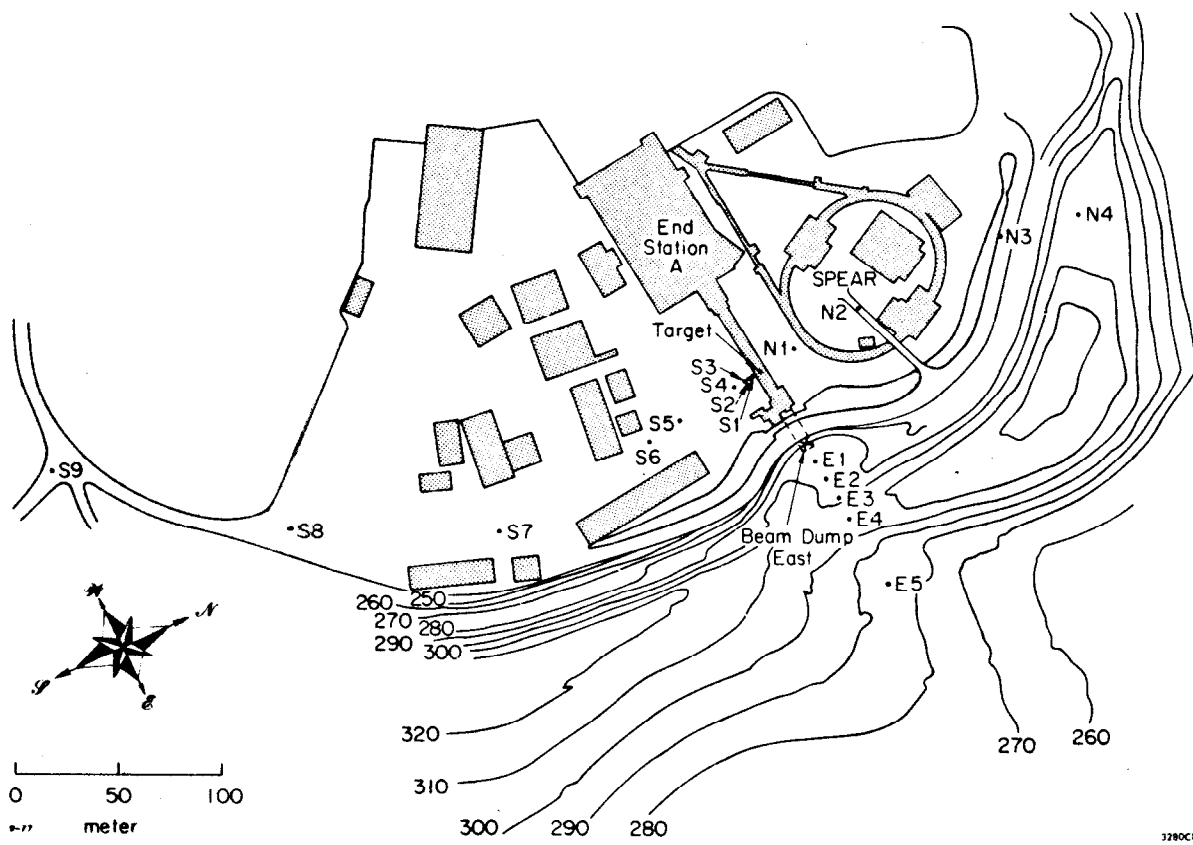
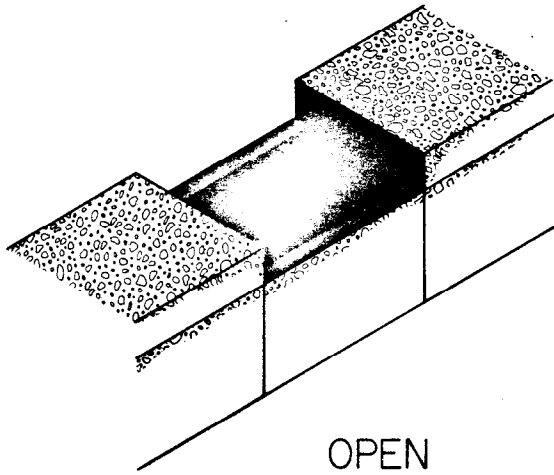


Fig. 3

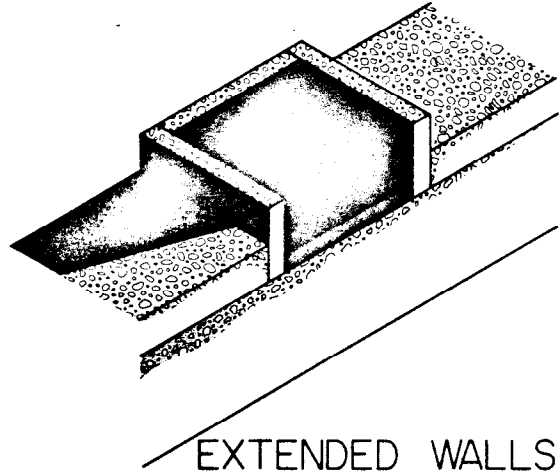


3280C1

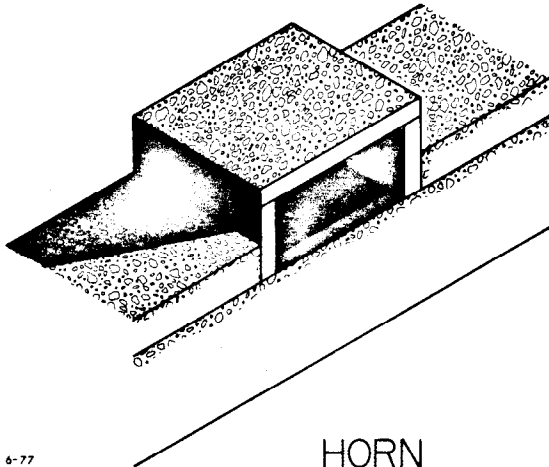
Fig. 4



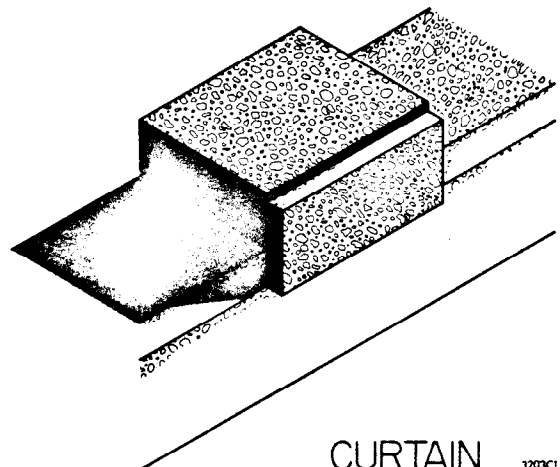
OPEN



EXTENDED WALLS



HORN



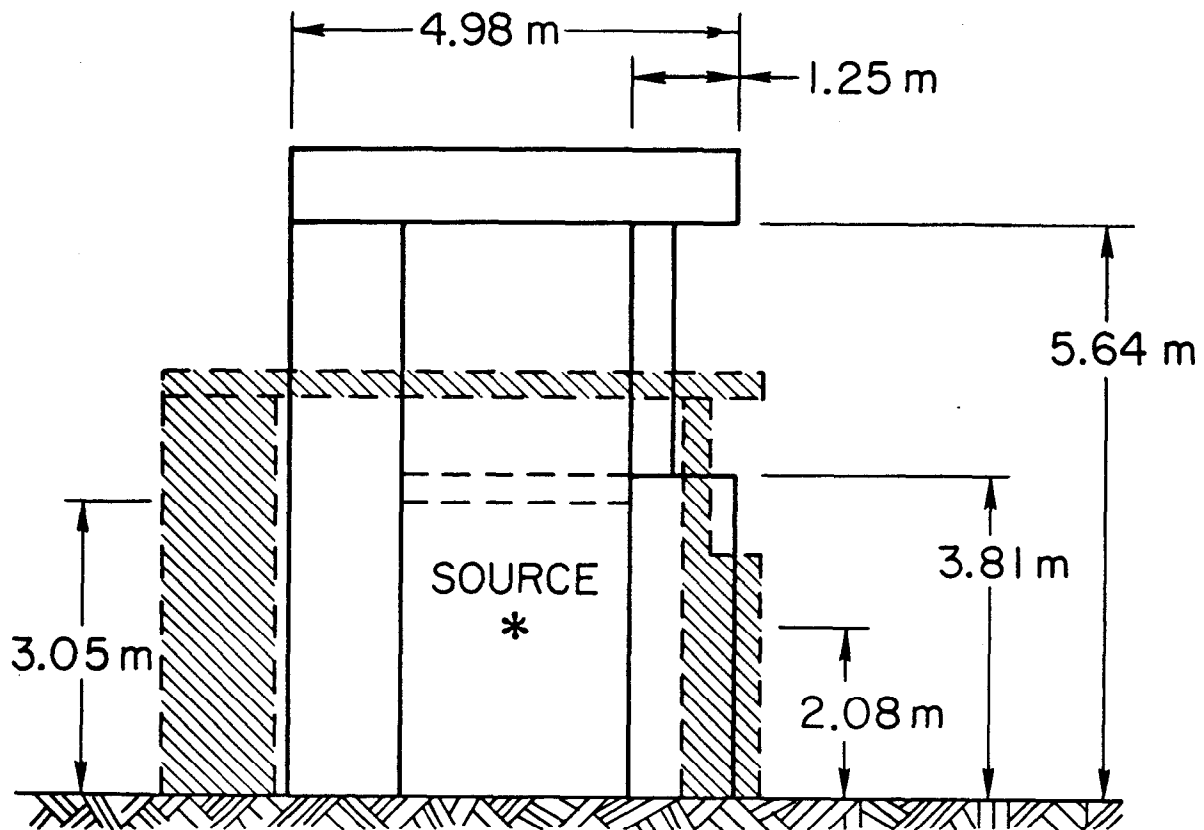
CURTAIN

6-77

3203C1

Fig. 5

▨ PEP IR (3x Scale of Mock up)
— ESA Mock up



5 - 78

333642

Fig. 6

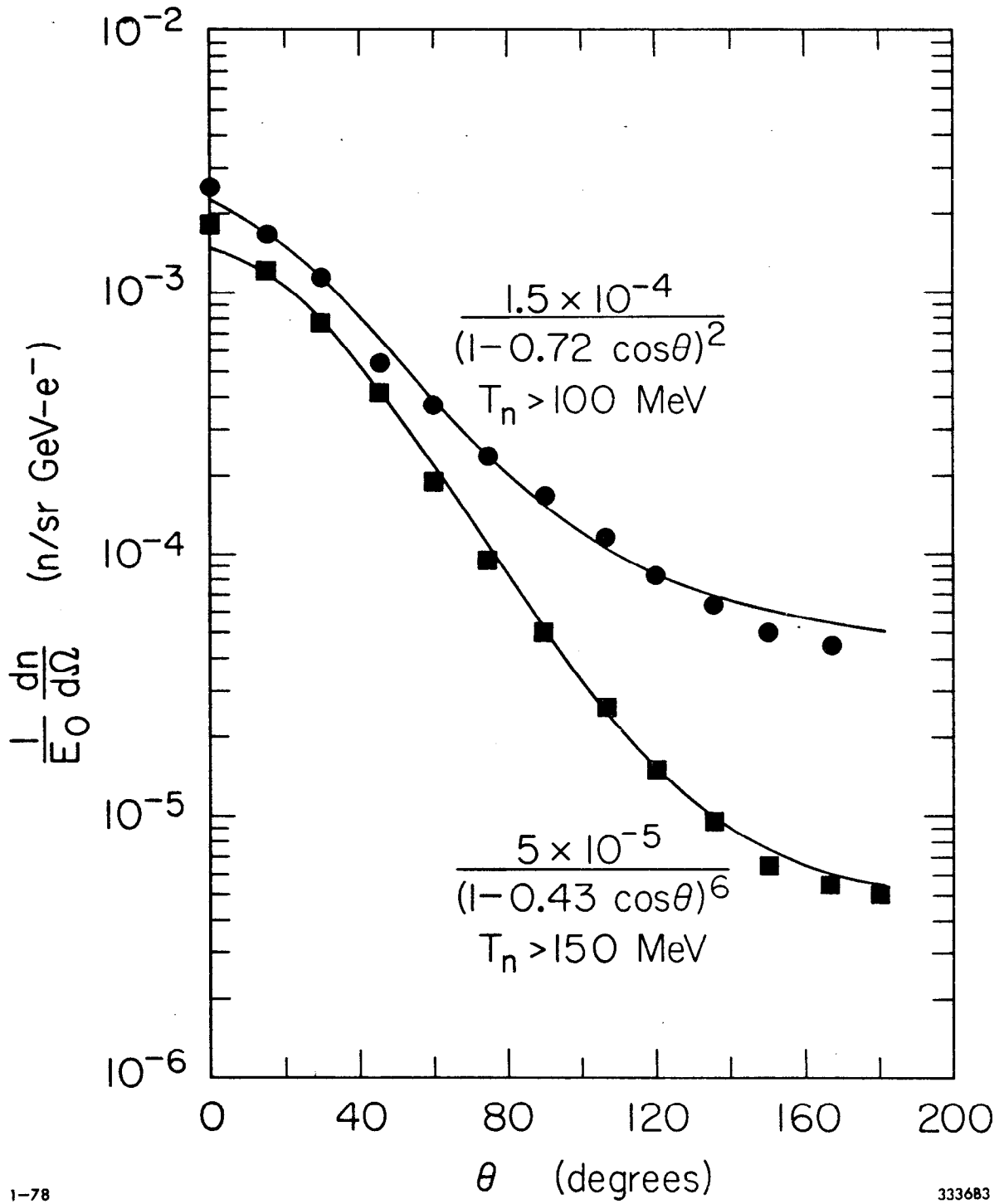


Fig. 7

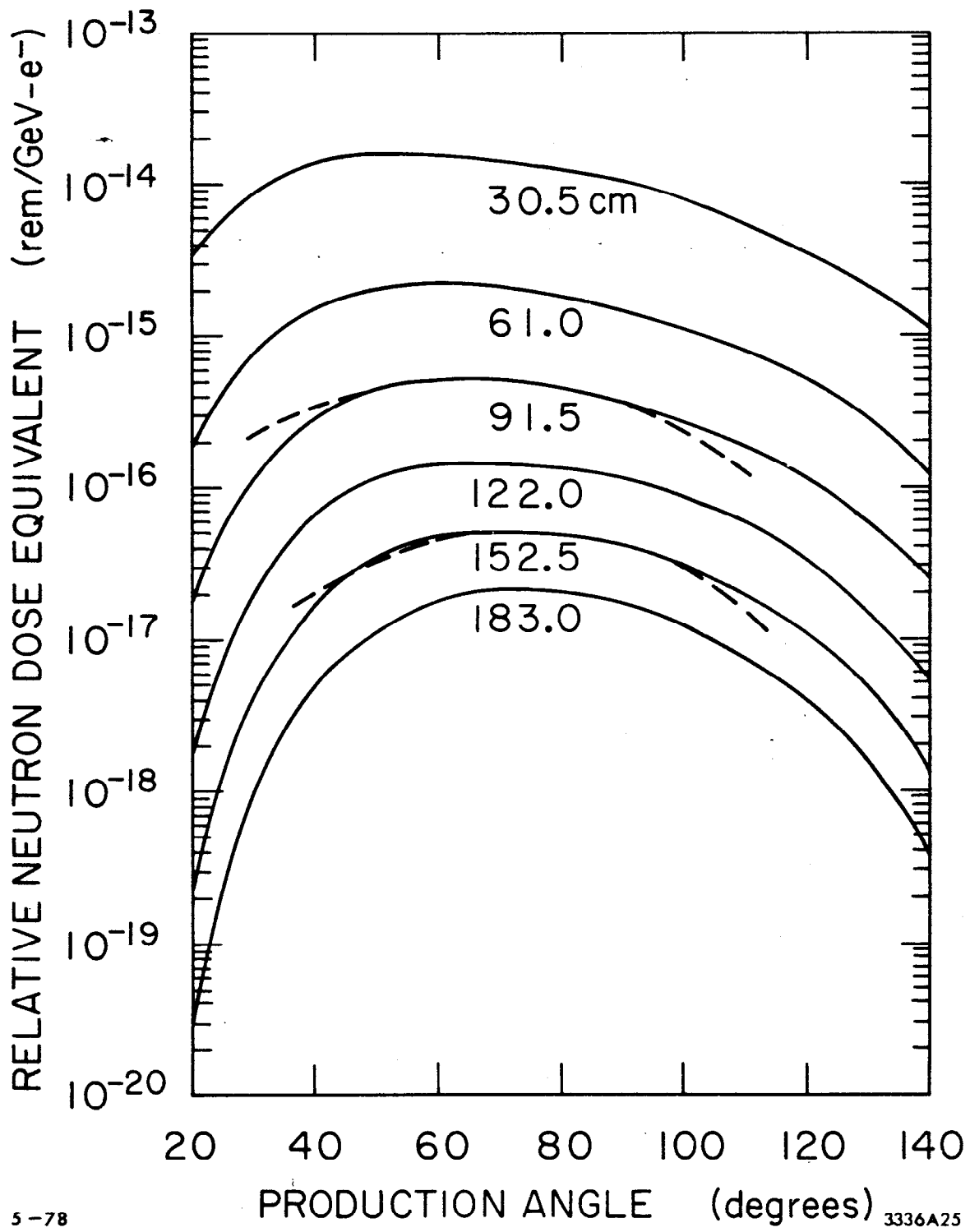


Fig. 8

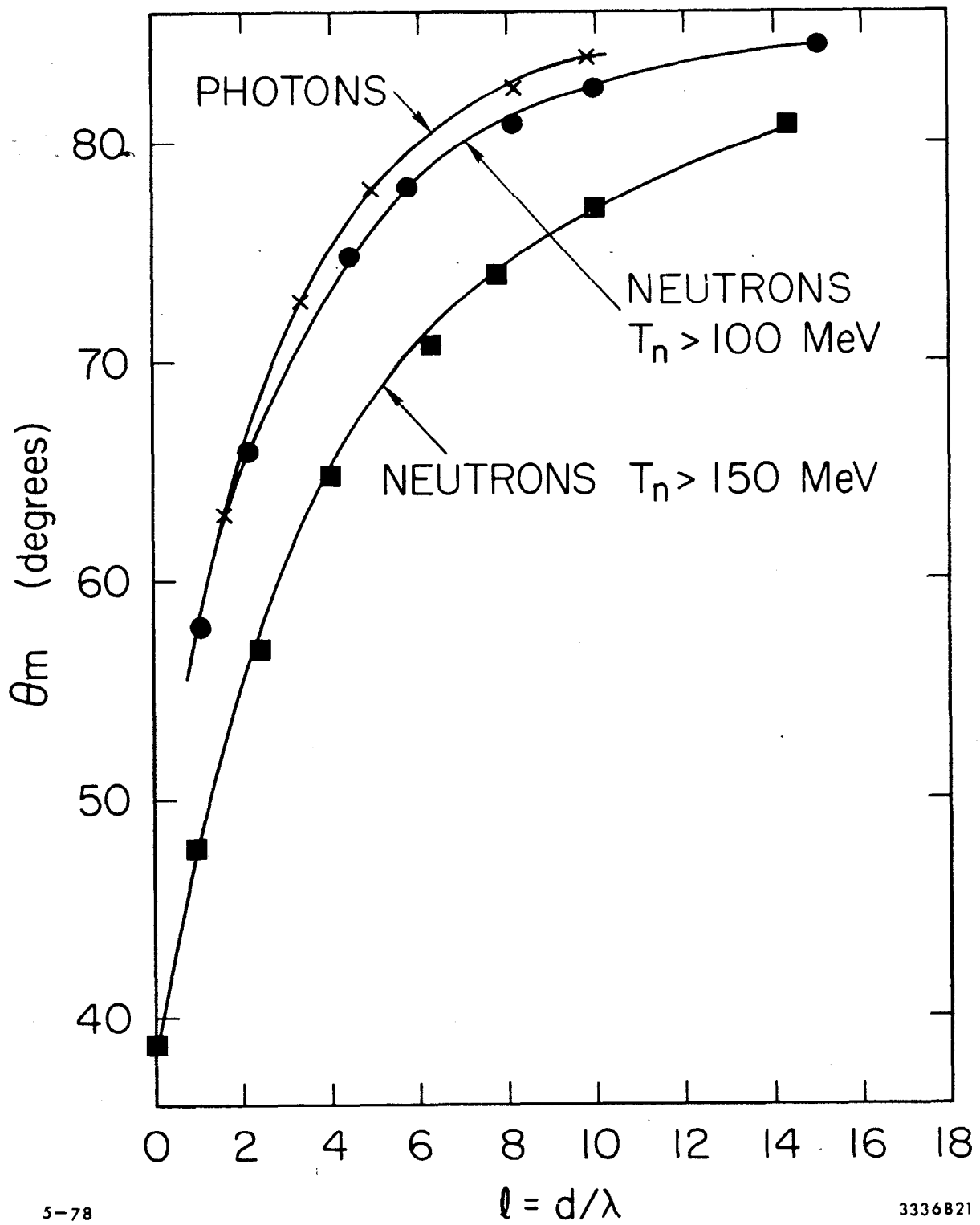
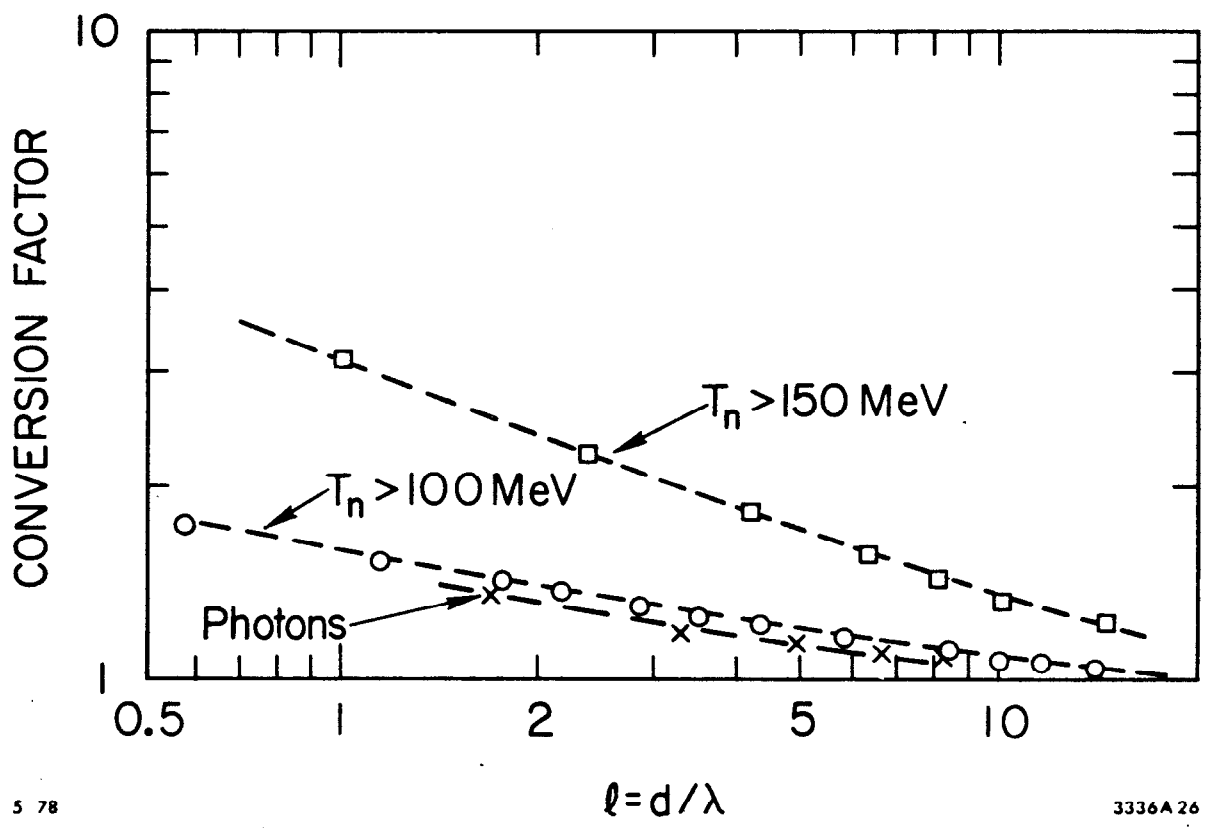
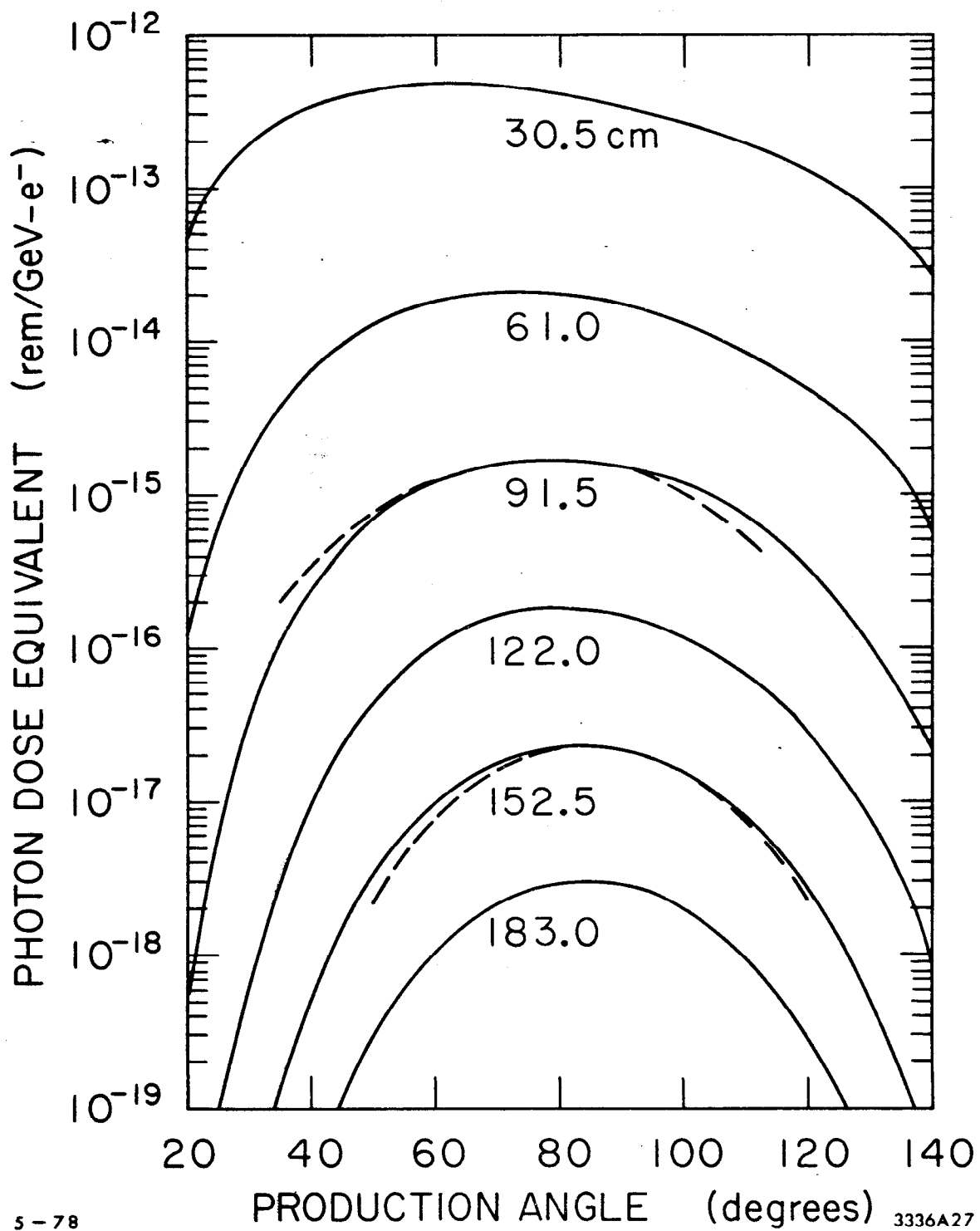


Fig. 9



$l = d/\lambda$

Fig. 10



5-78

3336A27

Fig. 11

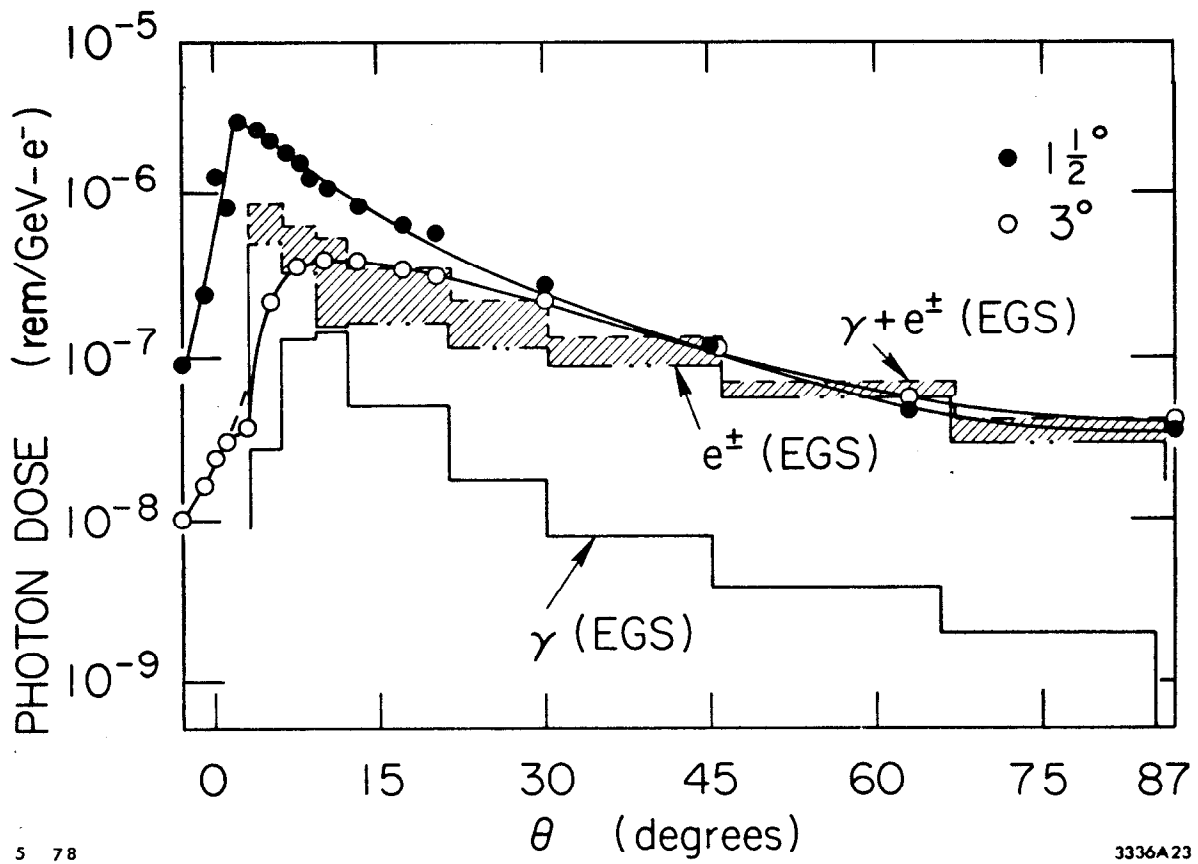


Fig. 12

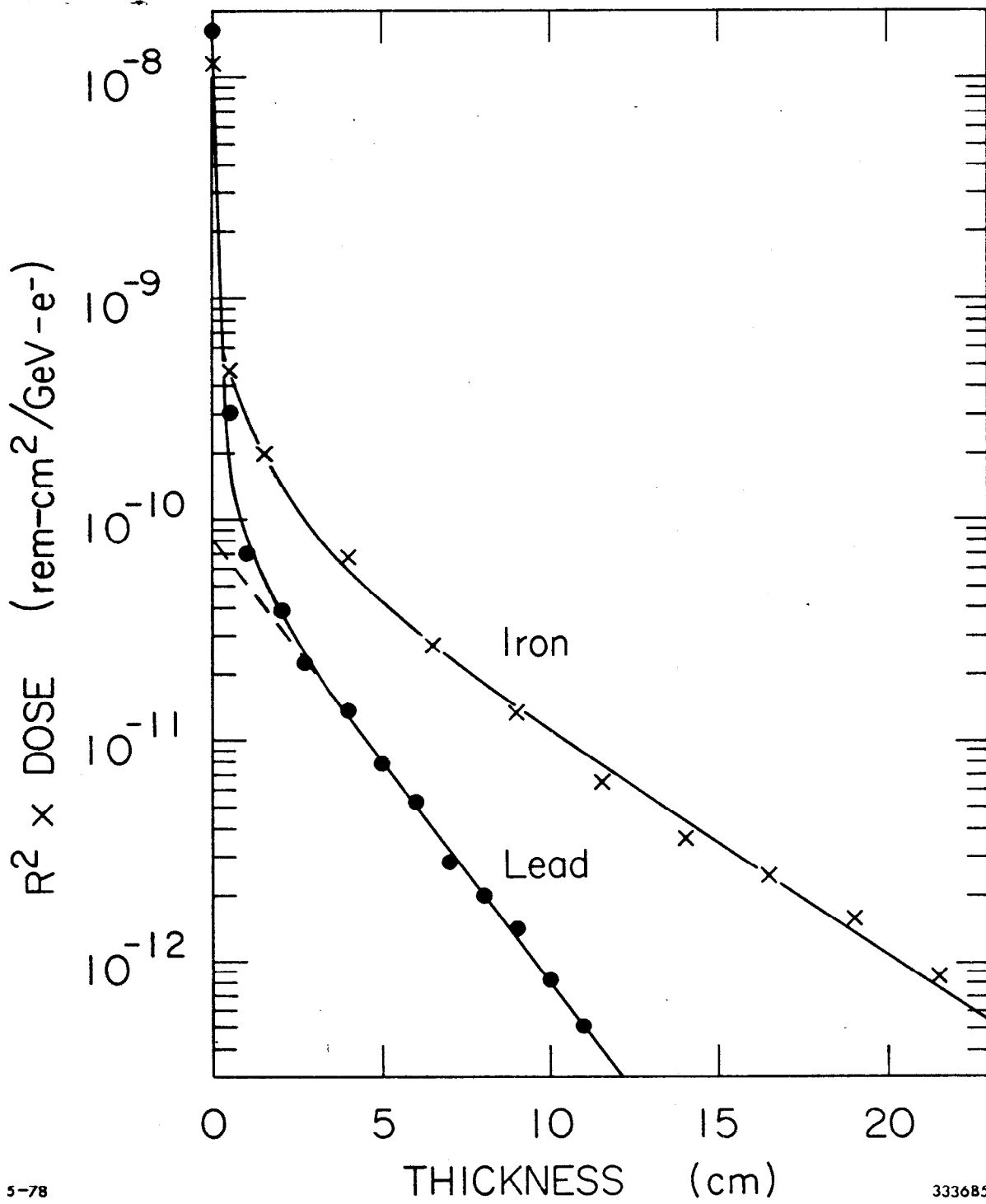


Fig. 13

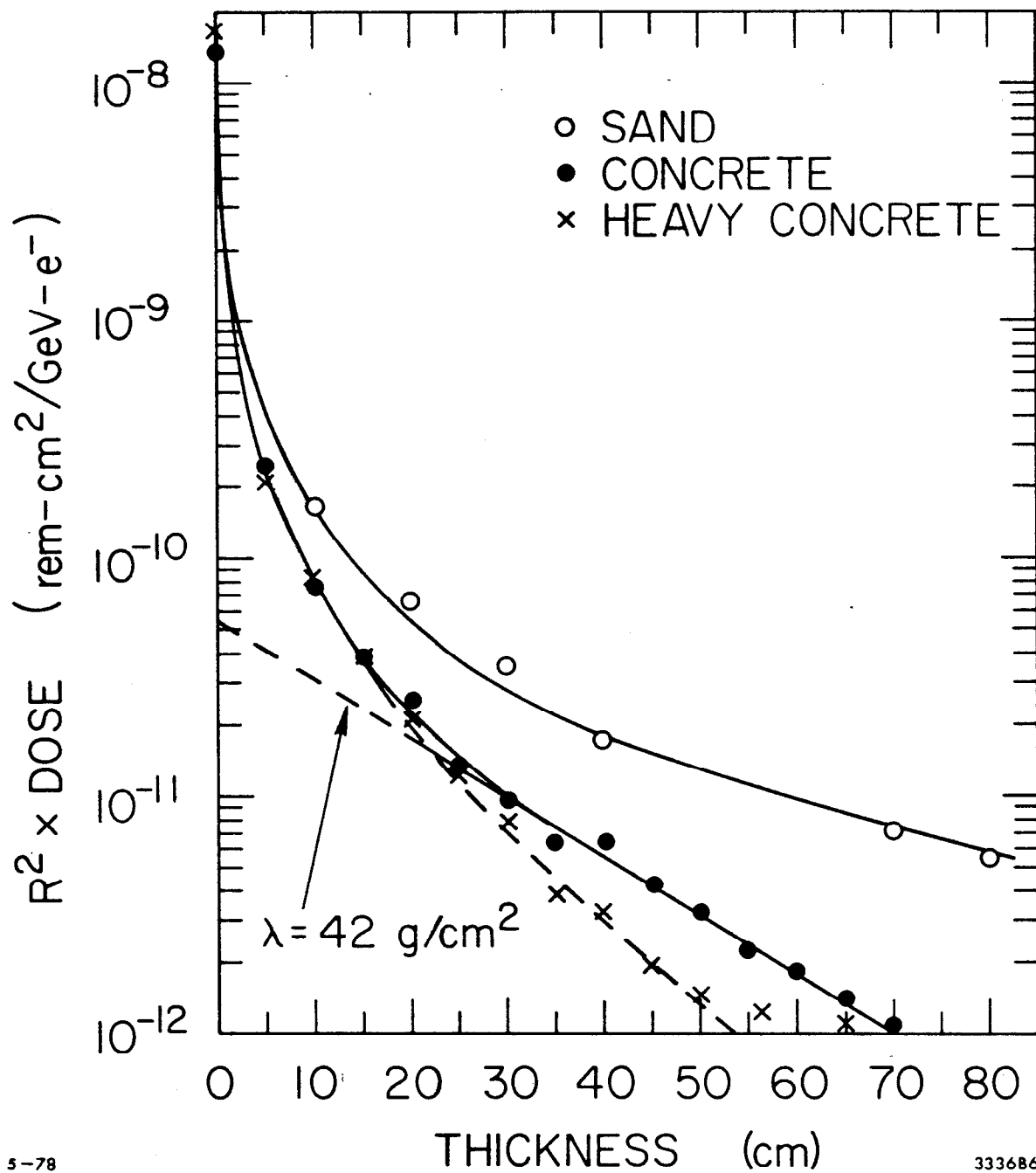


Fig. 14

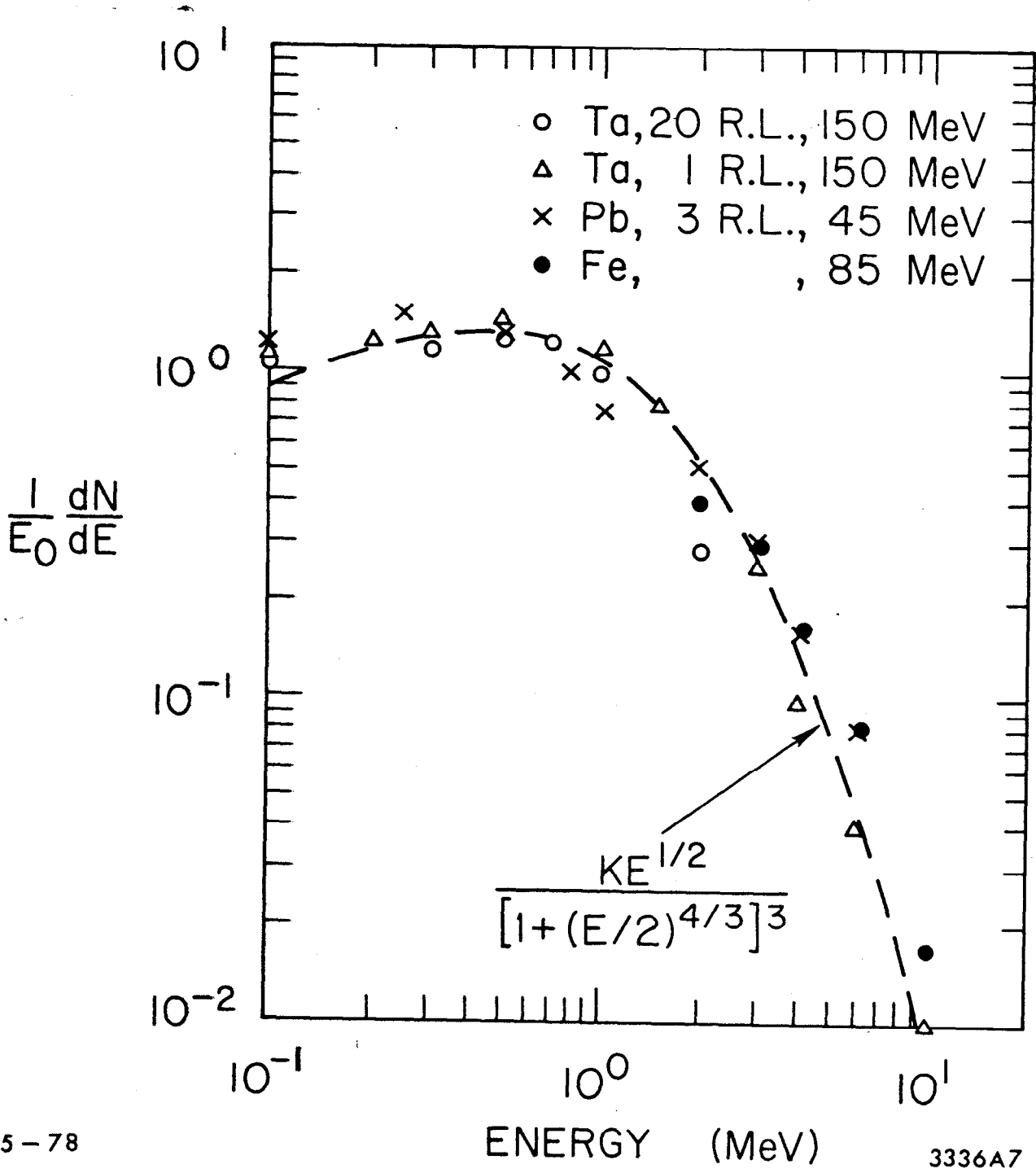


Fig. 15

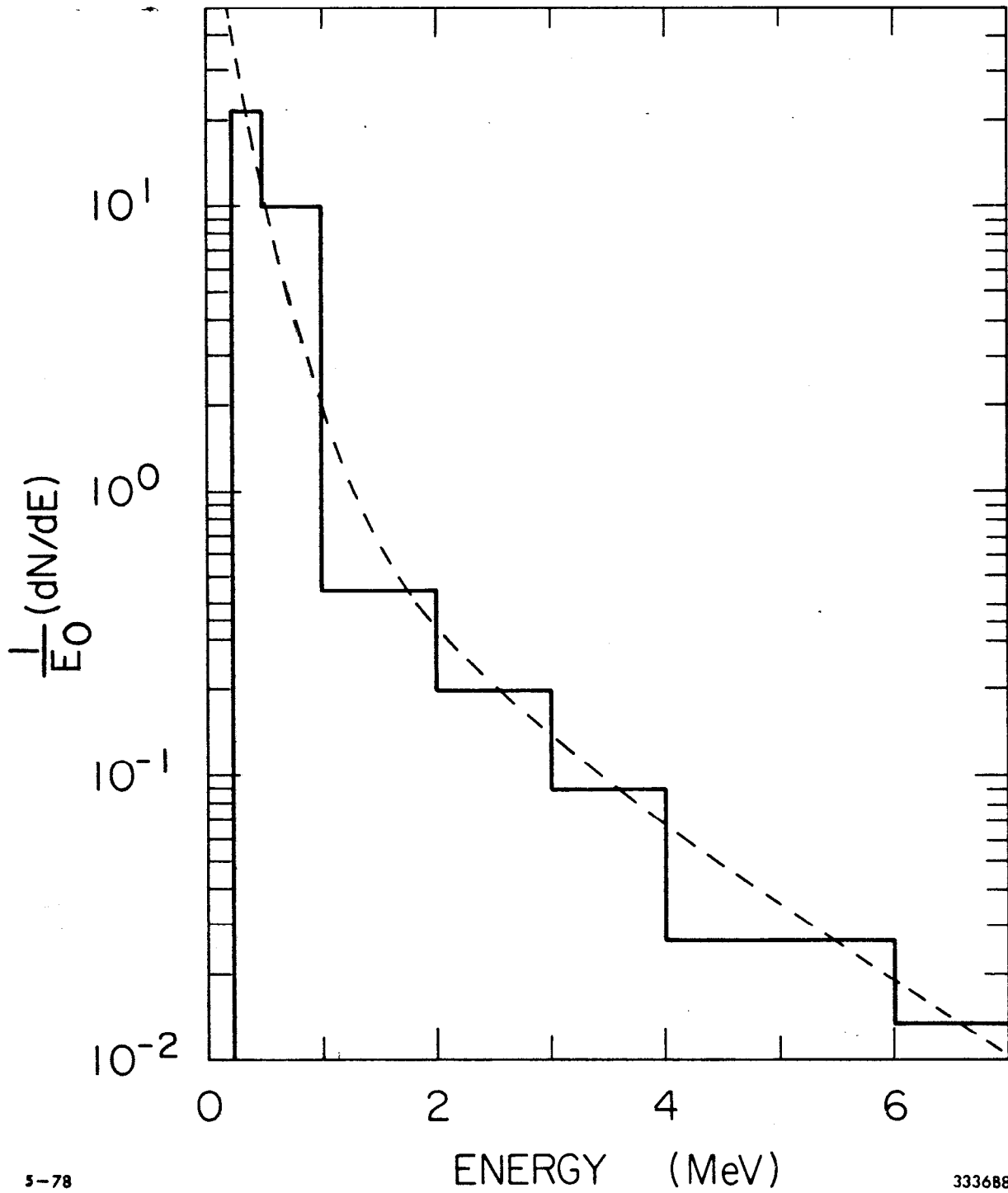


Fig. 16

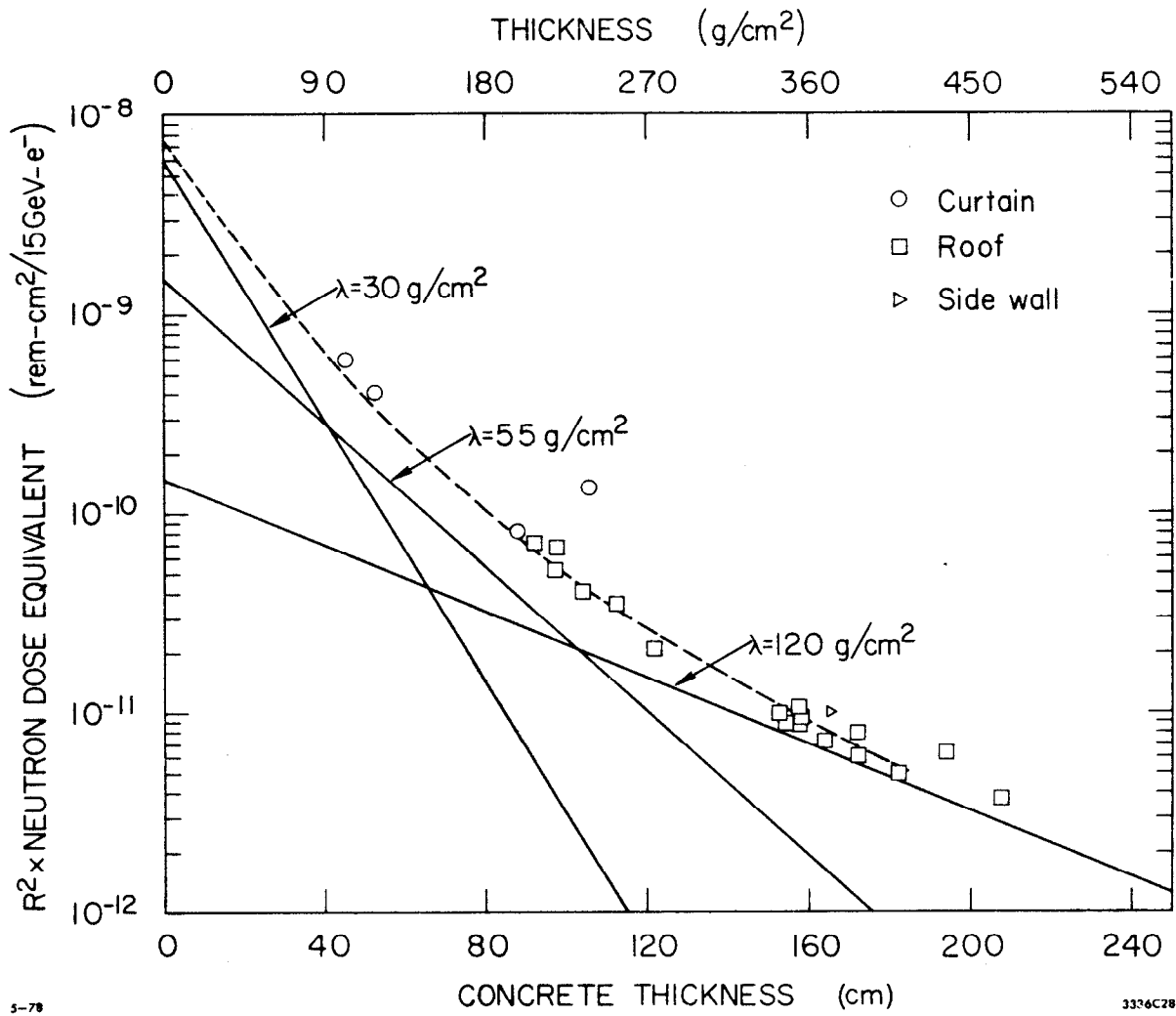


Fig. 17

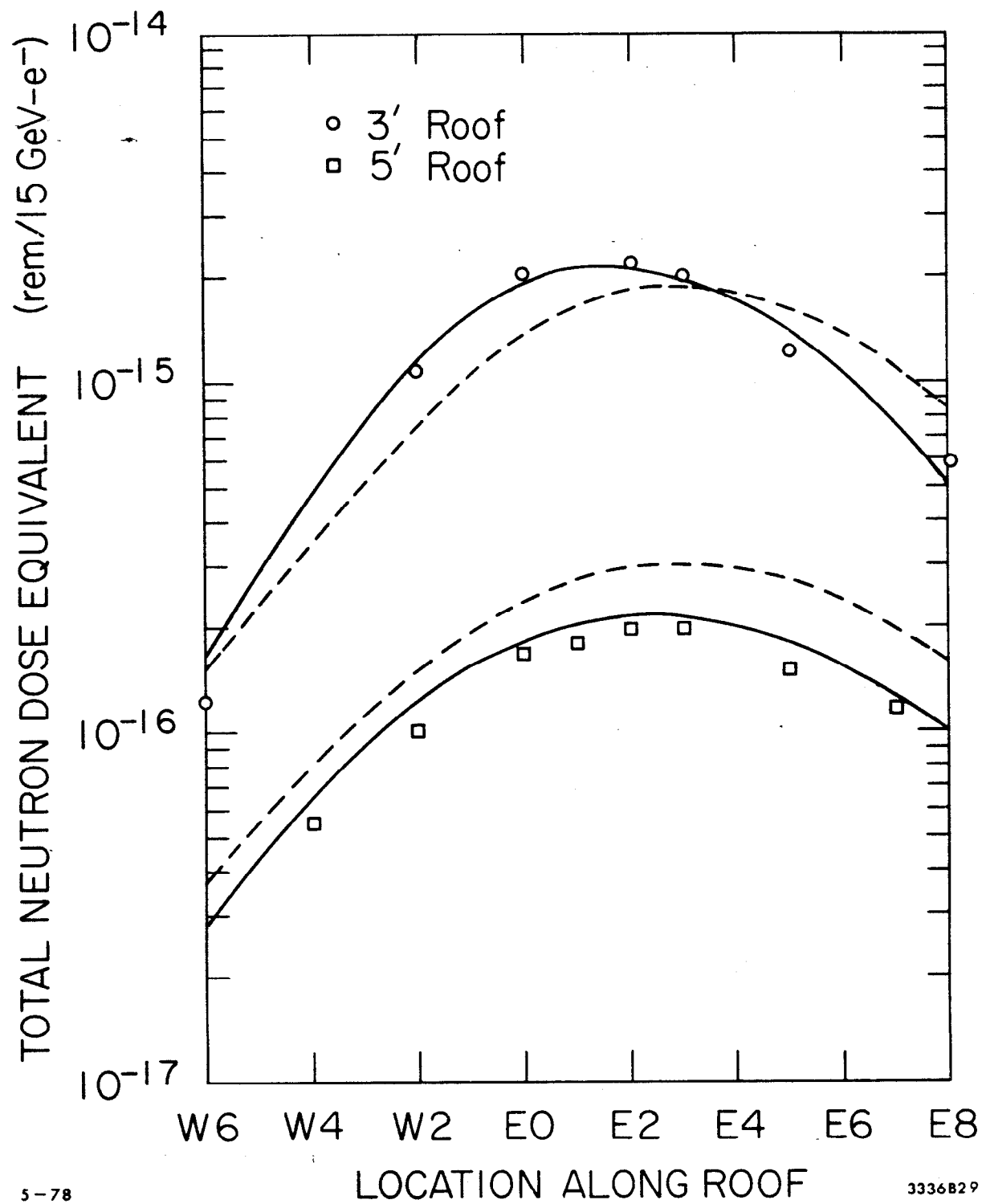


Fig. 18

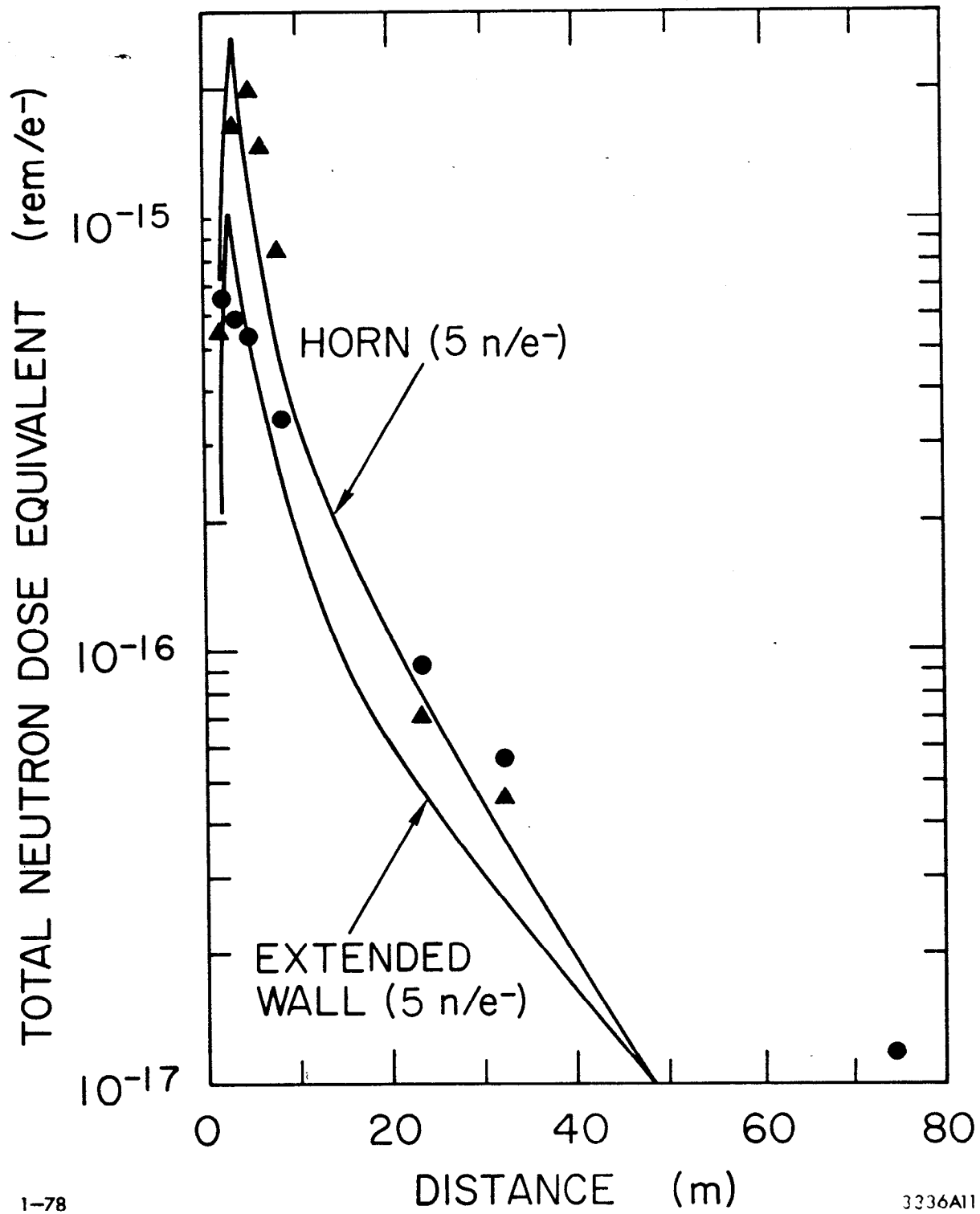


Fig. 19

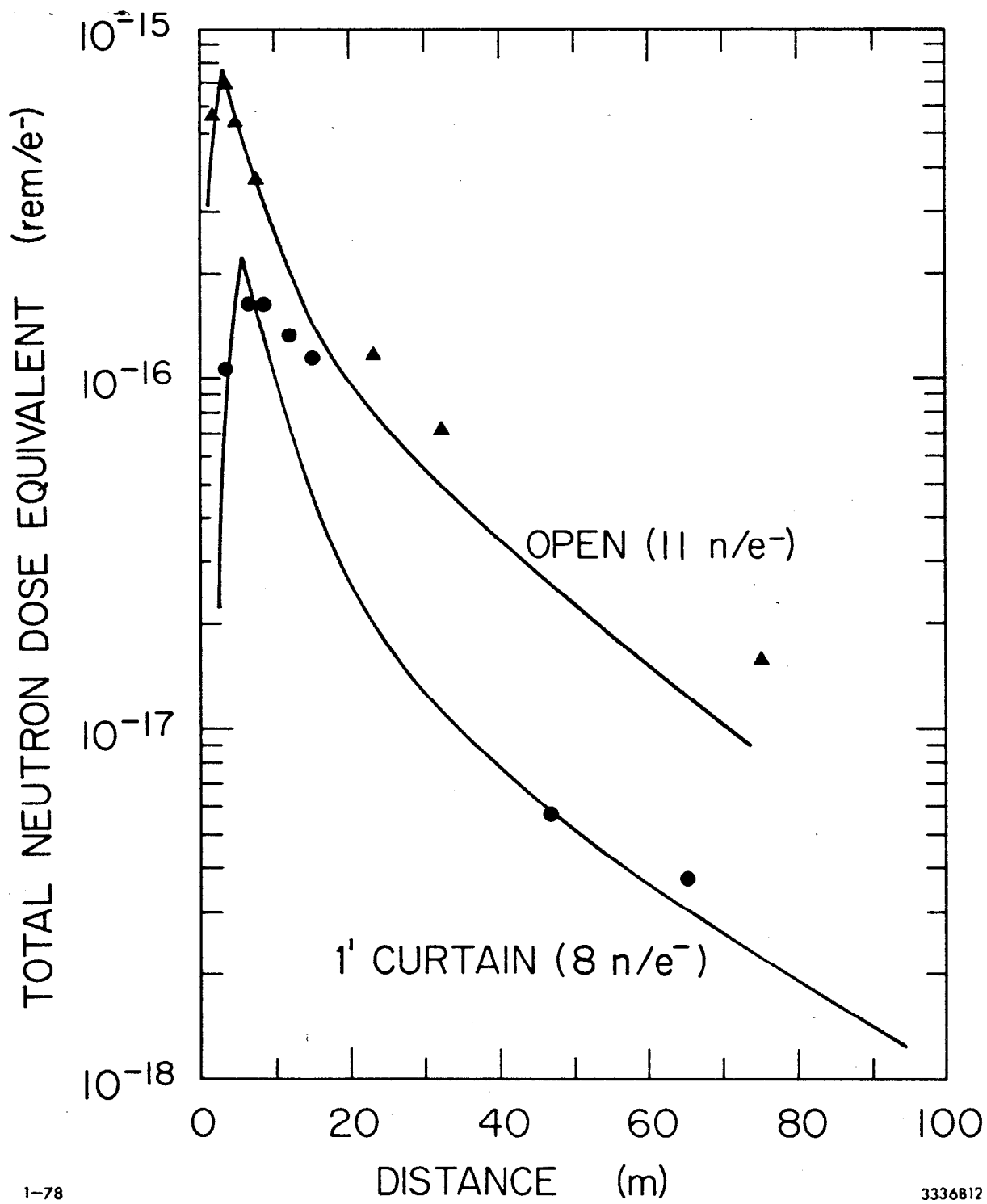


Fig. 20

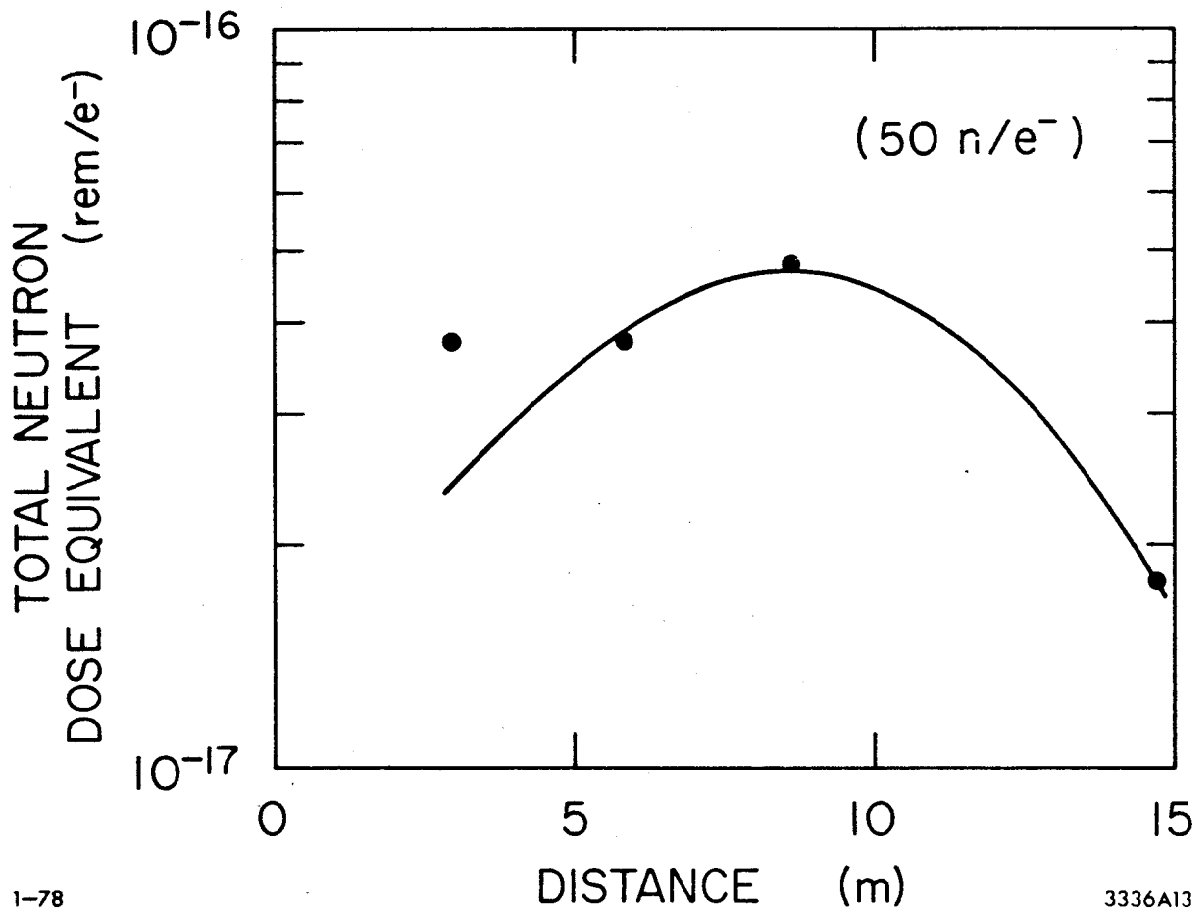


Fig. 21

TOTAL NEUTRON DOSE EQUIVALENT (rem/15 GeV-e⁻)

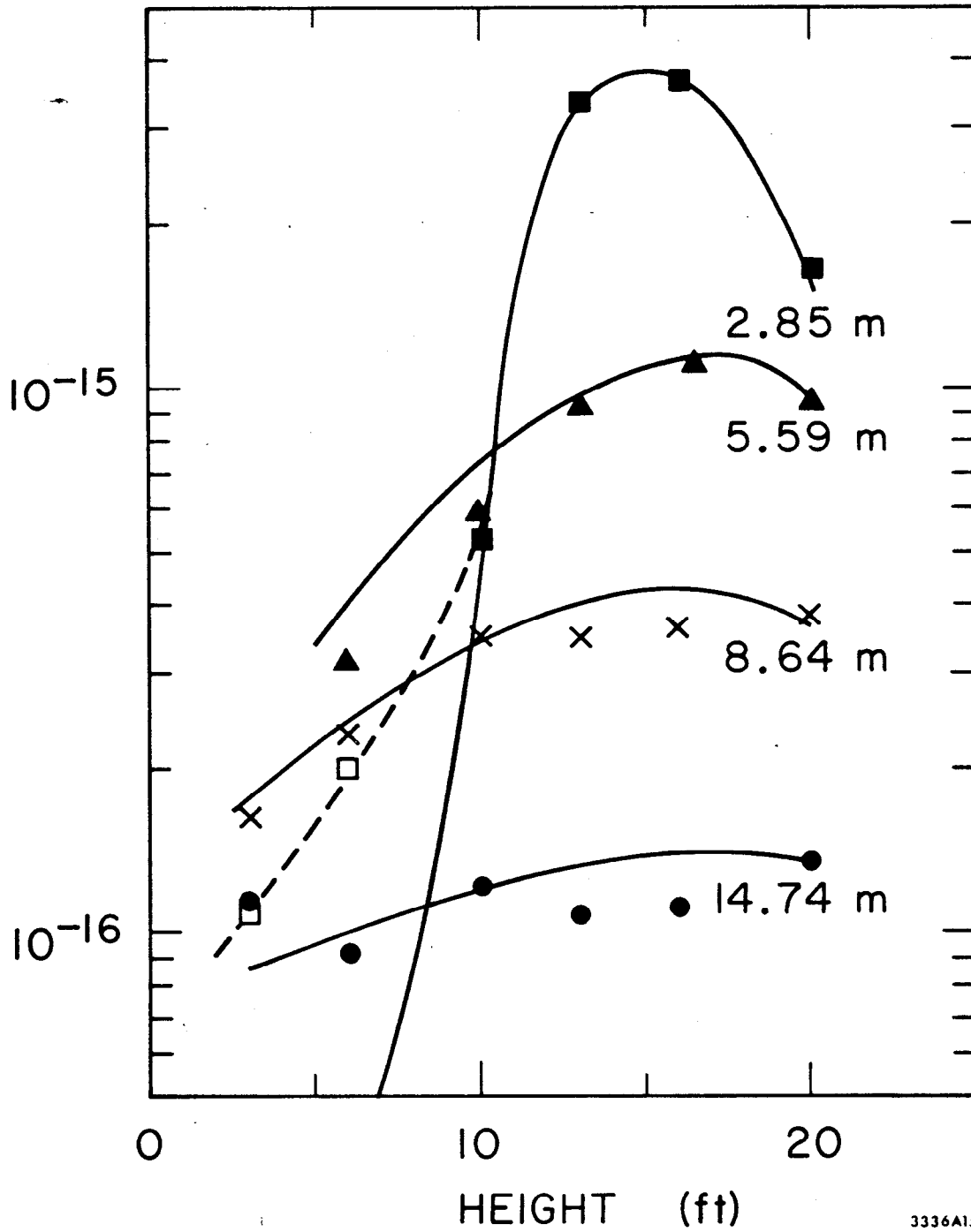


Fig. 22

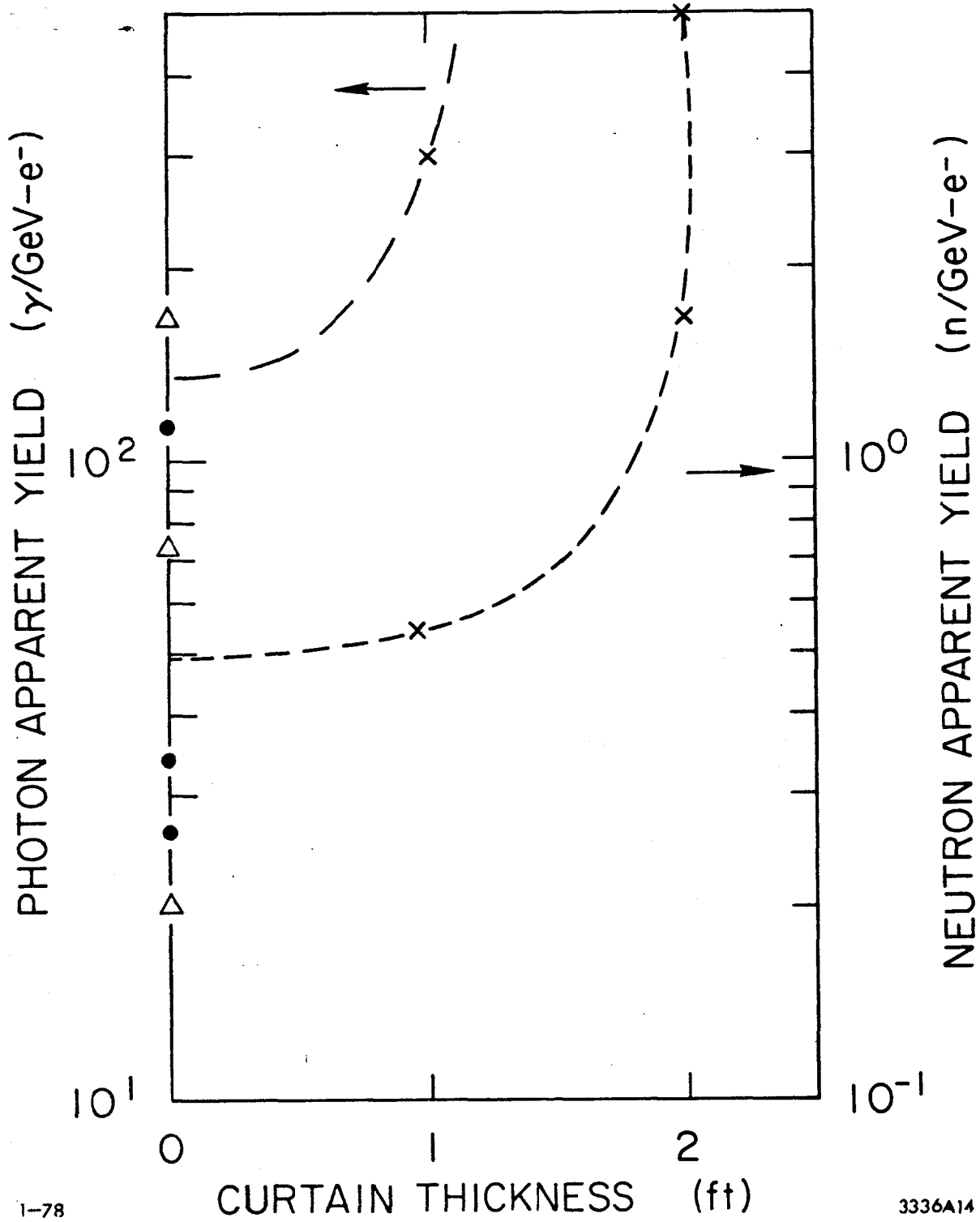


Fig. 23

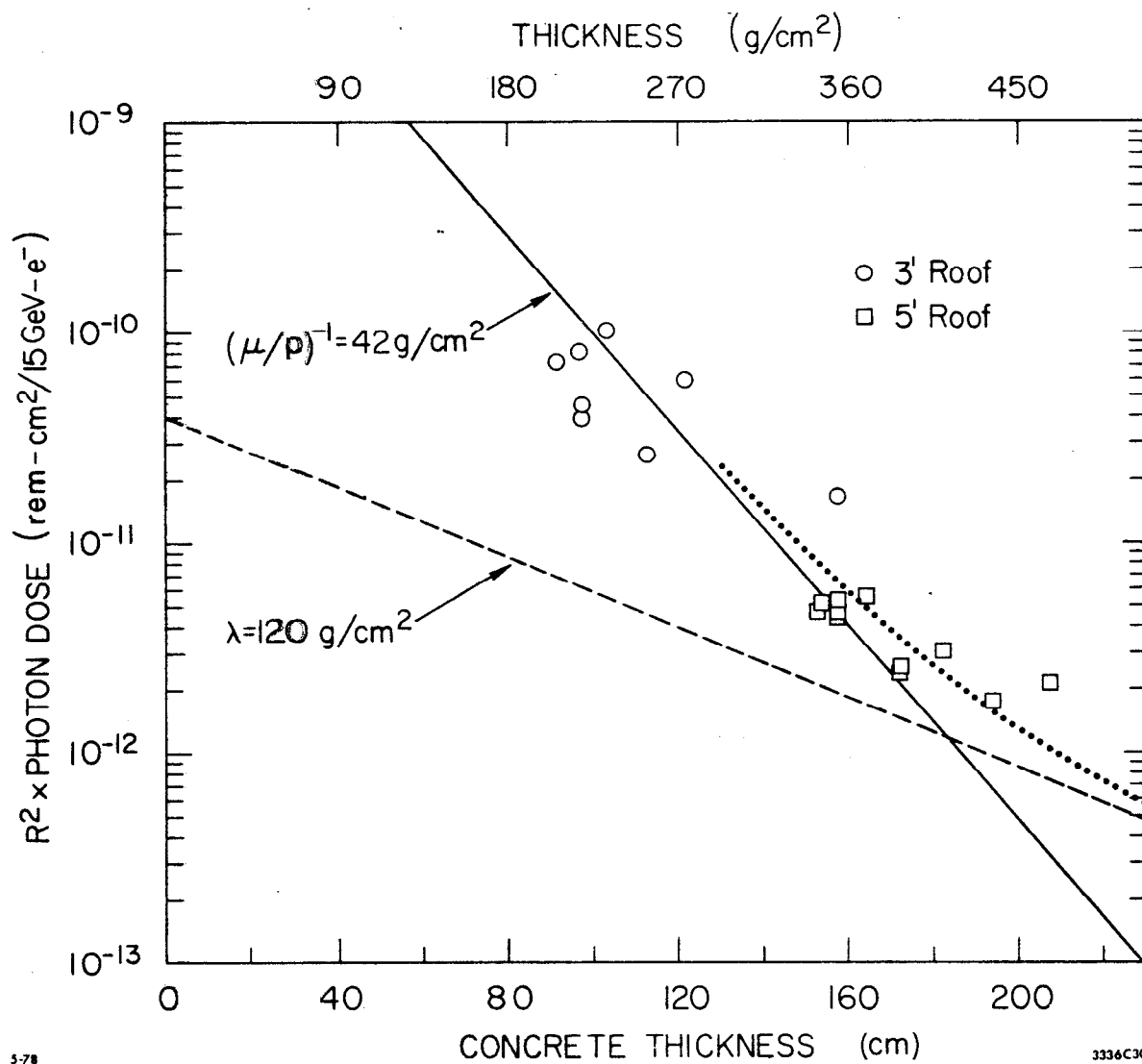


Fig. 24

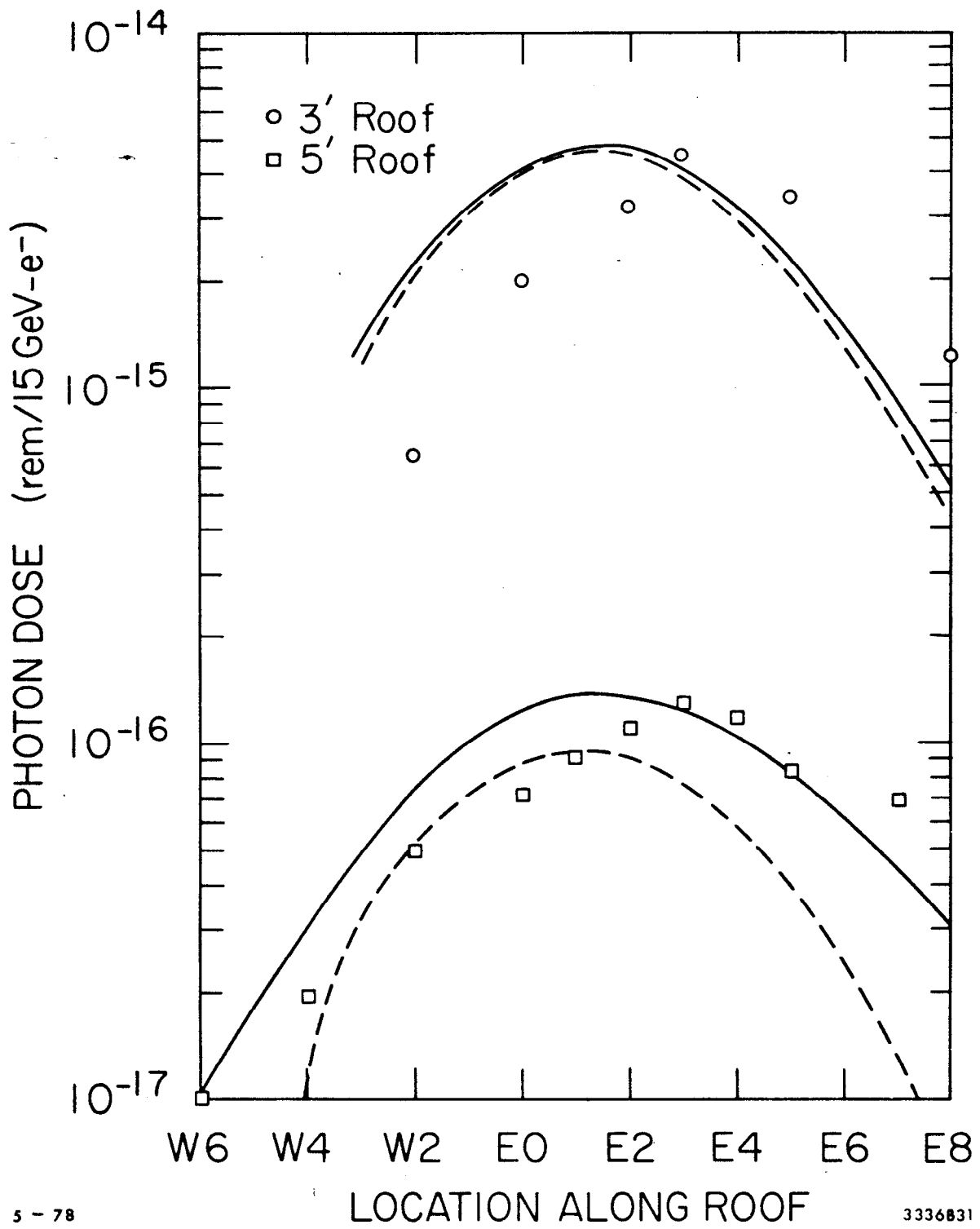


Fig. 25

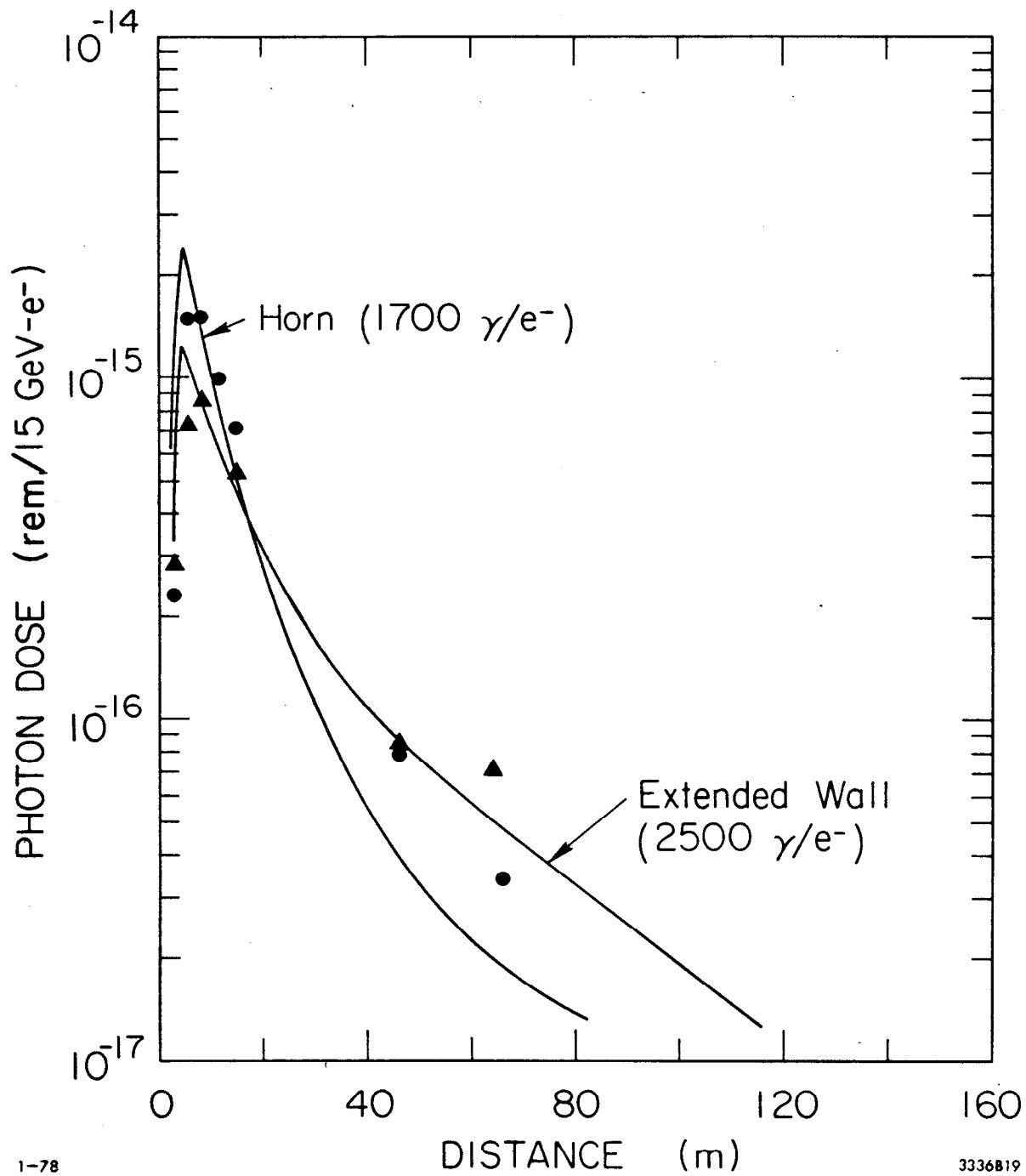


Fig 26

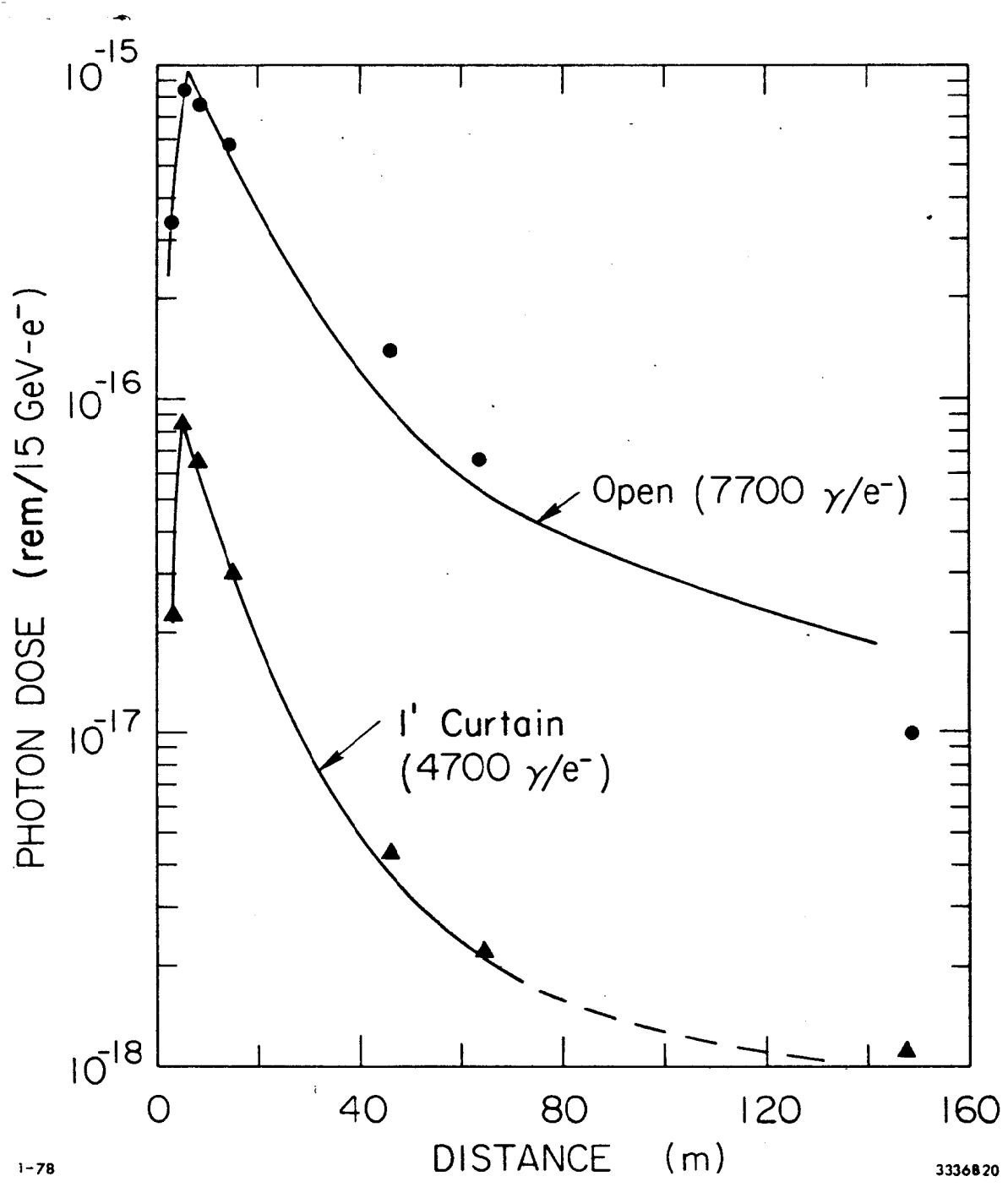


Fig. 27

APPENDIX A

Some Expanded Remarks on Neutrons

DeStaebler early coined the phrase 'Method of Moyer' (DE62) to describe some of the simplifications used in the shielding of the original 20 GeV electron accelerator at SLAC. This was in reference to Moyer (MO61) who used the fact that the neutron inelastic cross sections are essentially constant above 100-150 MeV and that the lower energies have attenuation lengths considerably shorter, to ignore all energies below 100-150 MeV, and to use a constant value for the removal mean-free path. If the reader detects some equivocation on the choice of energy region where the cross section becomes constant, 100 or 150 MeV, it is intentional. Fig. 1A (PA73) shows inelastic cross sections; the choice of 100 MeV would seem appropriate. At the same time, many authors have referred to the value of 150 MeV (PA73) as being a convenient lower energy limit. The difference in yields for neutrons with energies, T_n , greater than 100 and 150 MeV as seen in Fig. 7, is considerable, especially at the larger production angles which makes the choice of either 100 or 150 MeV quite important for shielding at a high-energy electron accelerator.

The value of 100 MeV has always been used at SLAC. DeStaebler has fit the yield of neutrons with energies greater than 100 MeV with the analytic expression

$$\frac{1}{E_0} \frac{dN}{d\Omega} = \frac{1.5 \times 10^{-4}}{(1 - 0.72 \cos \theta)^2} \quad \text{n/sr-GeV-e} \quad (\text{A1})$$

The yields in Eqn. A1 are for a copper target and will change as the target material changes. Table 1 allows for target yield adjustment with material change.

TABLE 1

Material	Relative High Energy Neutron Yield
Aluminum	1.87
Iron	1.08
Copper	1.00
Lead	0.50

The value of the removal mean-free path for HEN's is proportional to $A^{1/3}$, where A is the atomic mass ($\lambda \approx 38 A^{1/3}$) (PA73), allowing for scaling λ to other elements.

2. Giant Resonance Neutrons (GR)

There's a sizeable uncertainty in the correct value of λ to use for neutrons in the G.R. energy range, as pointed out by Patterson and Thomas (PA73) who noted published values that varied by as much as a factor of 200. For fission neutrons, Price, et al (PR57) fit the removal cross section to an expression of the form of $0.21A^{-0.58} \text{ cm}^2/\text{g}$, which for concrete would be about 31.5 g/cm^2 .

APPENDIX B

Comments on Dead Times

Dead times of the neutron counters were covered quite well by ASH, et al, and it is not the intention to repeat them here. However, before that paper, dead times were corrected in a more simple (and less accurate) manner. This came from measurements of the arrival time of thermal neutrons to the actual BF_3 detector inside the moderator measured in 1964 and included in the text on accelerator shielding by Patterson and Thomas (PA73). This simplified correction was to assume a uniform arrival time equal to the time that roughly half the total thermal neutrons reached the detector. Then

$$R(\text{actual}) = R(\text{observed}) / (1 - R(\text{observed}) \times T(\text{effective})) \quad (\text{B1})$$

where $T(\text{effective},)$ is the effective system dead time for a pulsed machine given by

$$T(\text{effective}) = T(\text{electronic}) / (\text{rep. rate} \times \text{arrival time}) \quad (\text{B2})$$

$T(\text{electronic})$ is the system resolution time and the arrival time is the mean moderation time in the detector moderator which we have simplified to a constant.

Our original choice of a mean moderation time, based solely upon the arrival time of half the total number of neutrons arriving at the BF_3 detector inside the moderator, was 130 microseconds. We would expect this number to change when examined in light of actual measurement data such as we had from the fixed-location reference BF_3 , in conjunction with independent measurement of the system resolution time. This was done for the Nov BF_3 data with a value of T , the mean moderation time, determined to be 175 microseconds. Actually, as was pointed out by Ash, et al, when one observes the fall-off in observed count

rate with increasing expected count rate, what is really measured is the ratio of t/T , system resolution-to-moderation time. For the Nov runs, he tabulated the Ref BF_3 t/T to be 71.9 which would give a value of T of about 141 microseconds. For the Dec runs, Ash, et al, gives values of t/T of 73.3 for the BF_3 and 13.6 for the rem counter.

(Counter sensitivities and system resolution times were different for the Nov and Dec runs.)

Using an arrival time of 175 microseconds and the measured system dead time gives results that are everywhere within 10% of the values given by Ash, et al, for the Dec ESA-PEP measurements.

APPENDIX C

Comments on Location Symbols

There may have been some ambiguity in the report by Ash, et al, (AS77) as to the symbols used to designate location. Quite simply, every location is preceded by a letter which is a compass point. For those measurements made on the roof, the number following the letter stands for the distance, in feet, from a point directly above the beam targeting position. For example, E3 would be a point 3 feet to the east of the target center (where the target point was assumed to be beneath E_0), while N4 would be 4 feet to the north. Beam direction was from west to east. For the side measurements, the letters again refer to compass points, but the numbers following have no physical meaning. Instead, one must look at the column headed 'dist', which will be the horizontal distance from source to that location. Thus S4, for example, indicates a point to the south of the target location at a distance of 14.74 meters from the source as listed in the 'dist' column. The locations labeled with the compass point, S, and a number between 1 and 3 followed by a 9 and then numbers between 3 and 20 stand for measurements 90° south of the target point at heights above the ground from 3 feet to 20 feet. For example, S4 9 16 refers to the south location S4, which is located at a horizontal distance of 14.64 meters from the source 90° to the target, and at a height of 16 feet above the ground. Note that the distance given in the 'dist' column is the horizontal distance to the S4 location only and not the actual source-to-detector distance for a detector 6 feet off the ground at S4.

APPENDIX D

Some Input Parameters Used in MORSE

Tissue Response Functions Used in MORSE

Neutron Upper Energy Boundary (MeV)	$\Delta E \times \text{rem/n/cm}^2$	Neutron Upper Energy Boundary (MeV)	$\Delta E \times \text{rem/n/cm}^2$
19.6	4.27×10^{-8}	1.8	3.86×10^{-8}
16.9	4.21×10^{-8}	1.1	2.89×10^{-8}
14.9	4.21×10^{-8}	5.5×10^{-1}	1.50×10^{-8}
14.2	4.21×10^{-8}	1.6×10^{-1}	7.12×10^{-9}
13.8	4.15×10^{-8}	1.1×10^{-1}	4.96×10^{-9}
12.8	4.15×10^{-8}	5.2×10^{-2}	2.78×10^{-9}
12.2	4.15×10^{-8}	2.5×10^{-2}	1.85×10^{-9}
11.1	4.15×10^{-8}	2.2×10^{-2}	1.32×10^{-9}
10.0	4.08×10^{-8}	1.0×10^{-2}	9.92×10^{-10}
9.0	4.08×10^{-8}	3.4×10^{-3}	9.92×10^{-10}
8.2	4.08×10^{-8}	1.2×10^{-3}	9.92×10^{-10}
7.4	4.08×10^{-8}	5.8×10^{-4}	9.92×10^{-10}
6.4	4.08×10^{-8}	1.0×10^{-4}	9.92×10^{-10}
5.0	4.08×10^{-8}	2.9×10^{-5}	9.92×10^{-10}
4.7	4.08×10^{-8}	1.1×10^{-5}	9.92×10^{-10}
4.1	4.03×10^{-8}	3.1×10^{-6}	9.92×10^{-10}
3.0	4.00×10^{-8}	1.1×10^{-6}	9.92×10^{-10}
2.4	4.00×10^{-8}	4.1×10^{-7}	9.92×10^{-10}
2.3	3.97×10^{-8}		

Gamma Response Functions Used in MORSE

Photon Upper Energy Boundary (MeV)	$\Delta E \times \text{Rad/Photons/cm}^2$	Photon Upper Energy Boundary (MeV)	$\Delta E \times \text{Rad/Photons/cm}^2$
14.0	2.81×10^{-9}	1.0	4.15×10^{-10}
10.0	2.32×10^{-9}	0.7	2.81×10^{-10}
8.0	2.04×10^{-9}	0.45	1.85×10^{-10}
7.0	1.83×10^{-9}	0.30	9.26×10^{-11}
6.0	1.63×10^{-9}	0.15	5.05×10^{-11}
5.0	1.42×10^{-9}	0.10	3.58×10^{-11}
4.0	1.22×10^{-9}	0.07	3.43×10^{-11}
3.0	1.04×10^{-9}	0.045	4.87×10^{-11}
2.5	9.02×10^{-10}	0.030	9.92×10^{-11}
2.0	7.51×10^{-10}	0.020	1.00×10^{-10}
1.5	5.73×10^{-10}		

Composition of Concrete Used in MORSE

(p = 2.26 g/cm³)

Element	Density
H	1.375×10^{-2}
O	4.587×10^{-2}
Al	1.743×10^{-3}
Si	2.015×10^{-2}
Ca	2.66×10^{-3}

REDUCED, CORRECTED, COMBINED AND AVERAGED DATA
FROM PEP SHIELDING TESTS AT 15 GEV *

1#ESAO OPEN CONFIGURATION

NOV 1976

N/S pts on line perpendicular to beam, 5 ft upstream of tgt.

E pts in vert. plane of beam line, downstream of tgt.

LOC	HGT	DIST	BF3	ER(%)	REM	ER(%)	ION	ER(%)
S1	3	2.9	0.17E-07	5.	0.34E-15	7.	0.34E-15	4.
S2	3	5.6	0.22E-07	5.	0.42E-15	7.	0.83E-15	4.
S3	3	8.6	0.21E-07	5.	0.33E-15	7.	0.77E-15	4.
S4	3	14.7	0.16E-07	5.	0.22E-15	7.	0.56E-15	4.
S5	3	45.8	0.48E-08	5.	0.71E-16	7.	0.13E-15	4.
S6	3	64.1	0.29E-08	3.	0.43E-16	6.	0.66E-16	4.
S7	3	149.5	0.72E-09	4.	0.97E-17	8.	0.10E-16	6.
S8	3	241.0	0.25E-09	4.	0.37E-17	12.	0.22E-17	25.
N1	3	19.8	0.11E-07	5.	0.21E-15	8.	0.36E-15	4.
N2	3	54.9	0.38E-08	5.	0.59E-16	7.	0.81E-16	4.
N3	3	134.2	0.11E-08	4.	0.16E-16	10.	0.15E-16	11.
N4	3	173.9	0.75E-09	4.	0.11E-16	12.	0.92E-17	17.
E1	3	51.9	0.39E-08	6.	0.85E-16	9.	0.44E-15	4.
E2	3	61.1	0.35E-08	6.	0.65E-16	9.	0.25E-15	4.
E3	3	73.2	0.24E-08	5.	0.31E-16	7.	0.15E-15	4.
E4	3	85.6	0.20E-08	5.	0.34E-16	7.	0.34E-16	4.
E5	3	122.2	0.97E-09	4.	0.11E-16	8.	0.16E-16	5.

1#ESAW WALL CONFIGURATION

NOV 1976

N/S pts on line perpendicular to beam, 5 ft upstream of tgt.

E pts in vert. plane of beam line, downstream of tgt.

LOC	HGT	DIST	BF3	ER(%)	REM	ER(%)	ION	ER(%)
S1	3	2.9	0.18E-07	7.	0.40E-15	23.	0.28E-15	9.
S2	3	5.6	0.20E-07	8.	0.36E-15	23.	0.74E-15	5.
S3	3	8.6	0.20E-07	7.	0.34E-15	22.	0.86E-15	5.
S4	3	14.7	0.18E-07	5.	0.21E-15	8.	0.53E-15	3.
S5	3	45.8	0.52E-08	4.	0.57E-16	7.	0.94E-16	3.
S6	3	64.1	0.26E-08	2.	0.35E-16	5.	0.72E-16	2.
S7	3	149.5	0.61E-09	4.	0.74E-17	14.	0.12E-16	7.
S8	3	241.0	0.20E-09	3.	0.39E-17	13.	0.14E-16	5.
N1	3	19.8	0.66E-08	5.	0.11E-15	9.	0.12E-15	4.
N2	3	54.9	0.21E-08	4.	0.31E-16	12.	0.23E-16	11.
N3	3	134.2	0.58E-09	4.	0.86E-17	20.	0.79E-17	25.
N4	3	173.9	0.40E-09	5.	0.24E-17	38.	0.41E-17	50.
E1	3	51.9	0.34E-08	4.	0.42E-16	11.	0.62E-16	5.
E2	3	61.1	0.25E-08	4.	0.35E-16	12.	0.39E-16	7.
E3	3	73.2	0.18E-08	4.	0.19E-16	14.	0.30E-16	7.
E4	3	85.6	0.14E-08	4.	0.16E-16	15.	0.19E-16	11.
E5	3	122.2	0.62E-09	5.	0.29E-17	38.	0.50E-17	50.

(E-2)

1#ESAH HORN CONFIGURATION

NOV 1976

N/S pts on line perpendicular to beam, 5 ft upstream of tgt.

E pts in vert. plane of beam line, downstream of tgt.

#CURTO SAME AS PREVIOUS "HORN" CONFIGURATION

DEC 1976

Pts on line perpendicular to beam, 5 ft upstream of tgt.

LOC	HGT	DIST	BF3	ER(%)	REM	ER(%)	ION	ER(%)
S1	3	2.9	0.21E-07	3.	0.33E-15	8.	0.30E-15	4.
S2	3	5.6	0.63E-07	3.	0.10E-14	7.	0.15E-14	3.
S3	3	8.6	0.67E-07	3.	0.12E-14	7.	0.15E-14	3.
S35	3	11.6	0.53E-07	4.	0.90E-15	9.	0.98E-15	7.
S4	3	14.7	0.38E-07	3.	0.51E-15	7.	0.78E-15	3.
S5	3	45.8	0.45E-08	5.	0.44E-16	9.	0.79E-16	4.
S6	3	64.1	0.18E-08	5.	0.28E-16	9.	0.34E-16	4.
S7	3	149.5	0.36E-09	4.	0.48E-17	15.	0.46E-17	13.
S8	3	241.0	0.11E-09	3.	0.19E-17	15.	0.22E-17	35.
N1	3	19.8	0.29E-08	5.	0.38E-16	10.	0.32E-16	6.
N2	3	54.9	0.88E-09	4.	0.11E-16	16.	0.90E-17	17.
N3	3	134.2	0.20E-09	5.	0.14E-17	41.	0.98E-17	17.

1#CURT2 2 FT THICK CURTAIN CONFIGURATION

DEC 1976

Points in plane perpendicular to beam, through target

LOC	HGT	DIST	BF3	ER(%)	REM	ER(%)	ION	ER(%)
S19	3	2.9	0.22E-08	4.	0.63E-16	6.	0.26E-16	4.
S19	6	2.9	0.28E-08	4.	0.80E-16	6.	0.38E-16	4.
S19	10	2.9	0.39E-08	4.	0.11E-15	5.	0.68E-16	3.
S19	13	2.9	0.11E-07	6.	0.26E-15	7.	0.17E-15	4.
S19	16	2.9	0.11E-07	5.	0.31E-15	6.	0.34E-15	3.
S19	20	2.9	0.14E-07	5.	0.33E-15	6.	0.28E-15	3.
S29	3	5.6	0.15E-08	5.	0.38E-16	8.	0.25E-16	5.
S29	6	5.6	0.20E-08	5.	0.49E-16	8.	0.32E-16	5.
S29	10	5.6	0.31E-08	5.	0.78E-16	7.	0.54E-16	4.
S29	13	5.6	0.43E-08	5.	0.11E-15	7.	0.86E-16	4.
S29	16	5.6	0.50E-08	6.	0.13E-15	7.	0.12E-15	4.
S29	20	5.6	0.56E-08	6.	0.13E-15	7.	0.15E-15	4.
S39	3	8.6	0.11E-08	5.	0.32E-16	8.	0.13E-16	7.
S39	6	8.6	0.14E-08	5.	0.31E-16	8.	0.20E-16	5.
S39	10	8.6	0.16E-08	5.	0.38E-16	8.	0.25E-16	5.
S39	13	8.6	0.20E-08	5.	0.49E-16	8.	0.41E-16	4.
S39	16	8.6	0.23E-08	5.	0.57E-16	7.	0.50E-16	4.
S39	20	8.6	0.24E-08	5.	0.54E-16	7.	0.56E-16	4.
S49	3	14.7	0.64E-09	5.	0.15E-16	11.	0.41E-17	17.
S49	6	14.7	0.67E-09	5.	0.14E-16	12.	0.86E-17	9.
S49	10	14.7	0.75E-09	5.	0.15E-16	12.	0.88E-17	9.
S49	13	14.7	0.86E-09	5.	0.23E-16	10.	0.10E-16	8.
S49	16	14.7	0.90E-09	5.	0.24E-16	9.	0.16E-16	6.
S49	20	14.7	0.85E-09	5.	0.19E-16	10.	0.14E-16	6.

I/ESAC 1 FT THICK CURTAIN CONFIGURATION

NOV 1976

Pts on line perpendicular to beam, 5 ft upstream of tgt.

E pts in vertical plane of beam line, downstream of tgt.

#CURT1 1 FT THICK CURTAIN CONFIGURATION

DEC 1976

Points in perpendicular plane:

5 feet upstream of target for unsubscripted locations

Through target for "9" and "E" locations

10 feet upstream of target for "W" locations

LOC	HGT	DIST	BF3	ER(%)	REM	ER(%)	ION	ER(%)
S1	3	2.9	0.20E-08	2.	0.41E-16	4.	0.20E-16	4.
S1	6	2.9	0.22E-08	5.	0.49E-16	8.	0.15E-16	7.
S1	10	2.9	0.43E-08	5.	0.23E-15	6.	0.93E-16	3.
S1	13	2.9	0.41E-07	7.	0.95E-15	7.	0.44E-15	4.
S1	16	2.9	0.42E-07	4.	0.13E-14	6.	0.57E-15	3.
S1	20	2.9	0.24E-07	5.	0.71E-15	11.	0.49E-15	7.
S2	3	5.6	0.44E-08	4.	0.90E-16	5.	0.46E-16	3.
S3	3	8.6	0.48E-08	5.	0.73E-16	7.	0.53E-16	5.
S35	3	11.6	0.35E-08	5.	0.81E-16	7.	0.39E-16	5.
S4	3	14.7	0.27E-08	3.	0.45E-16	4.	0.30E-16	3.
S5	3	45.8	0.34E-09	4.	0.34E-17	12.	0.43E-17	13.
S6	3	64.1	0.12E-09	4.	0.22E-17	15.	0.22E-17	25.
S7	3	149.5	0.19E-10	5.	0.22E-18	32.	0.11E-17	50.
S8	3	241.0	0.58E-11	8.	0.89E-19	71.	0.11E-17	50.
N1	3	19.8	0.42E-09	4.	0.65E-17	13.	0.31E-17	50.
N2	3	54.9	0.92E-10	5.	0.15E-17	28.	0.29E-17	50.
E3	3	73.2	0.47E-10	6.	0.47E-18	50.	0.28E-17	50.
S19	3	2.9	0.31E-08	5.	0.64E-16	13.	0.25E-16	17.
S19	6	2.9	0.40E-08	4.	0.12E-15	9.	0.26E-16	16.
S19	10	2.9	0.15E-07	5.	0.32E-15	14.	0.10E-15	25.
S19	13	2.9	0.96E-07	5.	0.20E-14	7.	0.11E-14	5.
S19	16	2.9	0.86E-07	5.	0.22E-14	7.	0.23E-14	4.
S19	20	2.9	0.36E-07	5.	0.99E-15	9.	0.17E-14	4.
S29	3	5.6	0.45E-08	6.	0.10E-15	7.	0.47E-16	4.
S29	6	5.6	0.86E-08	4.	0.19E-15	5.	0.85E-16	3.
S29	10	5.6	0.18E-07	5.	0.35E-15	7.	0.18E-15	4.
S29	13	5.6	0.26E-07	6.	0.56E-15	7.	0.36E-15	4.
S29	16	5.6	0.26E-07	6.	0.66E-15	7.	0.46E-15	4.
S29	20	5.6	0.21E-07	5.	0.57E-15	7.	0.56E-15	4.
S39	3	8.6	0.50E-08	5.	0.10E-15	10.	0.43E-16	9.
S39	6	8.6	0.65E-08	5.	0.14E-15	9.	0.65E-16	7.
S39	10	8.6	0.82E-08	5.	0.21E-15	8.	0.89E-16	6.
S39	13	8.6	0.10E-07	5.	0.21E-15	8.	0.13E-15	5.
S39	16	8.6	0.11E-07	5.	0.22E-15	8.	0.17E-15	5.
S39	20	8.6	0.99E-08	5.	0.23E-15	8.	0.20E-15	4.
S49	3	14.7	0.27E-08	5.	0.69E-16	12.	0.22E-16	17.
S49	6	14.7	0.30E-08	5.	0.55E-16	13.	0.30E-16	13.
S49	10	14.7	0.31E-08	5.	0.74E-16	12.	0.29E-16	13.
S49	13	14.7	0.36E-08	5.	0.65E-16	12.	0.44E-16	9.
S49	16	14.7	0.36E-08	5.	0.67E-16	12.	0.51E-16	8.
S49	20	14.7	0.35E-08	5.	0.82E-16	11.	0.58E-16	7.

(E-4)

1#TOP1 3 FT THICK TOP CONFIGURATION

DEC 1976

+DIST=lines running E/W and N/S on top of roof shield.

LOC	HGT	DIST	BF3	ER(%)	REM	ER(%)	ION	ER(%)
E8	13	8.0	0.13E-07	6.	0.35E-15	19.	0.12E-14	6.
E5	13	5.0	0.24E-07	5.	0.72E-15	13.	0.34E-14	4.
E3	13	3.0	0.41E-07	5.	0.12E-14	11.	0.45E-14	4.
E2	13	2.0	0.36E-07	5.	0.13E-14	11.	0.32E-14	4.
E0	13	0.0	0.39E-07	5.	0.12E-14	11.	0.20E-14	5.
W2	13	-2.0	0.25E-07	5.	0.67E-15	14.	0.65E-15	8.
N4	13	4.0	0.20E-07	5.	0.45E-15	14.	0.49E-15	8.
S2	13	-2.0	0.25E-07	5.	0.80E-15	11.	0.11E-14	5.
S4	13	-4.0	0.13E-07	5.	0.35E-15	17.	0.45E-15	9.

1#TOP2 5 FT THICK TOP CONFIGURATION

DEC 1976

+DIST=lines running E/W and N/S on top of roof shield.

LOC	HGT	DIST	BF3	ER(%)	REM	ER(%)	ION	ER(%)
E7	15	7.0	0.23E-08	5.	0.69E-16	9.	0.69E-16	5.
E5	15	5.0	0.30E-08	5.	0.88E-16	8.	0.84E-16	5.
E3	15	3.0	0.36E-08	4.	0.11E-15	6.	0.13E-15	3.
E2	15	2.0	0.39E-08	4.	0.12E-15	7.	0.11E-15	4.
E1	15	1.0	0.36E-08	5.	0.10E-15	8.	0.93E-16	4.
E0	15	0.0	0.32E-08	2.	0.97E-16	4.	0.74E-16	2.
W2	15	-2.0	0.23E-08	4.	0.60E-16	7.	0.51E-16	5.
W4	15	-4.0	0.12E-08	5.	0.34E-16	12.	0.20E-16	9.
W6	15	-6.0	0.49E-09	5.	0.18E-16	15.	0.98E-17	17.
W9	15	-9.0	0.17E-09	7.	0.64E-17	25.	0.33E-17	50.
N4	15	4.0	0.21E-08	5.	0.54E-16	10.	0.36E-16	6.
S2	15	-2.0	0.28E-08	4.	0.79E-16	7.	0.64E-16	4.
S4	15	-4.0	0.16E-08	5.	0.37E-16	11.	0.27E-16	7.

1#SID2 5 FT THICK TOP; MEASUREMENTS 3FT ABOVE GROUND;

DEC 1976

Pts on line perpendicular to beam, thru tgt for "A" lcns.

5 ft upstream of target for other locations

LOC	HGT	DIST	BF3	ER(%)	REM	ER(%)	ION	ER(%)
S1	3	2.9	0.72E-09	4.	0.26E-16	7.	0.89E-17	7.
S2	3	5.6	0.59E-09	3.	0.19E-16	5.	0.63E-17	7.
S3	3	8.6	0.30E-09	5.	0.75E-17	10.	0.34E-17	17.
S4	3	14.7	0.12E-09	5.	0.35E-17	15.	0.23E-17	25.
S1A	3	2.9	0.17E-08	5.	0.57E-16	6.	0.24E-16	5.
S2A	3	5.6	0.84E-09	4.	0.26E-16	7.	0.11E-16	6.
S3A	3	8.6	0.39E-09	4.	0.92E-17	10.	0.57E-17	11.
S4A	3	14.7	0.13E-09	5.	0.32E-17	15.	0.12E-17	50.

* UNITS:(per 15 GeV e); BF3 - n /sq. cm.; REM - rem; ION - R;
DIST - horiz dist from tgt in meters except for "TOP"
. lcns were unit is ft; HGT - height above ground, ft.